



Strength of vapour cloud explosions in a traffic environment: a numerical parametric study

Downloaded from: <https://research.chalmers.se>, 2026-05-14 10:37 UTC

Citation for the original published paper (version of record):

Lozano Mendoza, F., Johansson, M., Leppänen, J. et al (2026). Strength of vapour cloud explosions in a traffic environment: a numerical parametric study. *Open Engineering*, 16(1).
<http://dx.doi.org/10.1515/eng-2025-0162>

N.B. When citing this work, cite the original published paper.

Regular Articles

Fabio Lozano*, Morgan Johansson, Joosef Leppänen and Mario Plos

Strength of vapour cloud explosions in a traffic environment: a numerical parametric study

<https://doi.org/10.1515/eng-2025-0162>

Received July 5, 2025; accepted December 15, 2025;

published online January 13, 2026

Abstract: A vapour cloud explosion (VCE) is often deemed one of the most likely scenarios following an unintended release of flammable gas during road transport. Such VCEs produce a blast wave that propagates away from the explosion, potentially causing significant damage and loss of life. The severity of the generated blast loading depends on the VCE's strength. However, there is currently a noticeable lack of knowledge about the strength of VCEs on urban roads or related settings (such as carparks). This makes estimating the blast load characteristics challenging and imprecise. This study applied computational fluid dynamics to evaluate the strength of several VCE scenarios in a traffic environment. The scenarios consisted of groups of vehicles engulfed by a stoichiometric mixture of propane and air. The influence of parameters, such as the number of vehicles, the separation distance between vehicles, and the gas volume, was investigated using the principles of factorial design. The number of vehicles in the transverse direction had the most significant effect on the resulting overpressure. Indeed, the results indicated that this parameter alone may be sufficient for a conservative estimate of the strength of VCEs in a traffic environment.

Keywords: vapour cloud explosions; overpressure; TNO Multi-Energy Method; factorial design; FLACS-CFD

***Corresponding author: Fabio Lozano**, Division of Structural Engineering, Chalmers University of Technology, Gothenburg, SE-41296, Sweden, E-mail: lfabio@chalmers.se. <https://orcid.org/0000-0002-3935-4223>

Morgan Johansson, Division of Structural Engineering, Chalmers University of Technology, Gothenburg, SE-41296, Sweden; and Norconsult Sverige AB, Gothenburg, SE-41755, Sweden. <https://orcid.org/0000-0003-0020-0646>

Joosef Leppänen, Division of Structural Engineering, Chalmers University of Technology, Gothenburg, SE-41296, Sweden. <https://orcid.org/0000-0001-8620-8790>

Mario Plos, Swedish Transport Administration, Gothenburg, SE-41104, Sweden

1 Introduction

Although it may not be evident to the public, the transport of hazardous materials (hazmat) is common in modern society [1]. Hazmat include products that are flammable, explosive, poisonous, or possess other dangerous properties. Depending on the type of hazmat, an accidental release during transport may lead to catastrophic events such as explosions, fires, or toxic gas clouds. Among these tragic events, explosions arguably have the greatest potential to cause the greatest losses [2, 3]. Inland transport of hazmat is primarily conducted by road or railway, although the risk associated with road transport of hazmat is generally considered greater than that of rail transport, largely due to a lower accident rate in rail transport. Flammable gases are possible sources of explosions regularly transported by road. These are often transported in liquid state in pressurised vessels, such as liquefied petroleum gas (LPG), or in cryogenic vessels, such as liquefied natural gas (LNG). Explosive materials, such as TNT compositions and ammunition, may also be transported by road, although less frequently than flammable gases [4]. Potential scenarios following an unintended release of flammable gas include jet fires, flash fires, fireballs, and vapour cloud explosions (VCEs). Among these, a VCE is often regarded as the most likely event [5, 6].

A VCE is the combustion of a premixed mixture of flammable gas and air characterised by a rapid and major increase in overpressure and temperature [7]. The explosion sets the surrounding air into motion, which propagates as a blast wave. VCEs may result in substantial damage to property and loss of life. The accident in 2020 in Wenling, China [8–10], involving an unintended release of LPG from a road tanker, is a recent example of the tragic consequences of VCEs on urban roads. Hence, investigating the effects of VCEs in connection to hazmat transport by road is highly relevant.

In the event of a VCE on a road, nearby structures may be exposed to extreme loading conditions. However, while blast-resistant design of structures has been common for industrial facilities for decades, urban structures are historically seldom designed for load effects arising from accidental explosions. Nonetheless, the interest in blast-resistant design of urban structures has grown in recent years,

motivated by the increase in general awareness about explosion risks in traffic environments, coupled with the recent trend for urban densification (which means shorter distance between the road and the structures) and the rise of vehicles powered by alternative fuels (such as biogas or hydrogen) in some countries [11].

An essential part of evaluating the risk associated with VCEs in traffic environments is the accurate assessment of the strength of the explosion and the characteristics of the ensuing blast load. The term *traffic environment* is used in this article to refer to settings on or near a road where a group of vehicles is likely to be present in the event of an accidental release of a flammable gas during transport. Examples of traffic environments include congested roads, open carparks near the road, or refuelling stations. This article uses the term *strength* to refer to the overpressure generated by the explosion. The strength of a VCE strongly depends on the geometrical conditions of the environment in which it develops. In general, the combustion of vapour clouds in environments with a high degree of confinement (which limits free expansion of the flow) or obstruction (which promotes turbulence and flame acceleration) will result in stronger explosions. In open traffic environments, local areas that are partly confined and obstructed may exist due to the presence of vehicles. For instance, in the region under a group of vehicles, combustion largely develops in two-dimensional conditions. Furthermore, turbulence may be enhanced by the obstruction caused by the wheels and other components underneath the vehicles. Therefore, the degree of confinement and obstruction (and thus the resulting explosion strength) in open environments populated by vehicles depend on parameters such as the geometry of the vehicles, the number of vehicles, and the separation distance between vehicles.

Ideally, the estimation of the strength of VCEs would be based on experimental data. However, the availability of experimental research concerning VCEs in open traffic environments is currently limited. The experiment described in [12], designed to represent the explosion of a stoichiometric hydrogen–air mixture in a realistic refueling station, is a notable contribution. Instead, computational fluid dynamics (CFD) codes can be used to assess the strength of VCEs and the propagation of the resulting blast wave.

Several research studies concerned with evaluating the consequences of unintended releases of flammable gases employing CFD can be found in the literature. Most of the published work is concerned with risk evaluation and consequence analysis within the process industry, often combining dispersion and explosion analyses e.g. [13–15]. Some authors have also studied the prediction of blast waves arising from accidental explosions using CFD analysis

[16–18]. Shen et al. [19] compiled several examples of recent applications of CFD in the context of process safety, including 15 examples of VCEs. CFD has also been applied for evaluation of accidental explosions in urban settings [8, 20]. The studies by Venetsanos et al. [21, 22] are examples of early applications of CFD for investigating the release and explosion of a flammable gas in an urban environment. More recently, the development of graph neural networks has enabled their application for gas explosion prediction at an urban scale based on CFD simulations [23, 24]. Regarding implementation of CFD for traffic-related settings, two types of environments have garnered particular interest from the research community: vehicular tunnels [25–28] and refuelling stations [29–33], often concerning leakage, dispersion and explosion of mixtures containing hydrogen. However, very few examples of implementation of CFD for evaluation of explosions in open environments in which the vehicles are the main or only source of confinement and congestion are available.

For all their advantages, CFD codes have some drawbacks. Firstly, users must have specialised knowledge to utilise CFD codes correctly. Furthermore, CFD calculations are often time-consuming and may require high-performance computing. More importantly, CFD codes need to be validated against relevant experiments. Because of these aspects, CFD calculations may not be suitable in many circumstances, particularly in the early design phase or in situations in which many scenarios need to be evaluated. Therefore, there is a need for faster and simpler methods for estimating the strength of VCEs in a traffic environment and the characteristics of the blast load arising from the explosion.

A few simplified methods for estimating the blast load from VCEs have been developed based on experimental observations or numerical simulations. Examples of such methods include the TNO Multi-Energy Method (MEM) [34], the Baker-Strehlow-Tang (BST) method [35, 36], and the Congestion Assessment Method [37]. In all these methods, the user needs to make an estimate of the strength at the source of the blast based on the conditions of the scenario of interest. This is the most challenging aspect and the greatest source of uncertainty in such simplified methods. Guidelines for determining this parameter exist in the literature [38, 39]. Furthermore, some authors have proposed correlations to calculate the maximum overpressure for some specific conditions based on experiments or numerical analyses [40–42]. However, these guidelines have mostly been designed for applications in the chemical and process industry, making their implementation for explosion scenarios in traffic environments challenging and unprecise. Today, analysts are forced to adapt the existing guidelines to

traffic-related situations based on their own experience and judgement. This introduces an additional measure of subjectivity into the risk assessment process. As a result, the outcome of different risk analyses concerning VCEs in traffic environments with similar conditions may differ substantially, even within the framework of the same project [11]. Therefore, the prediction of the blast load generated by VCEs in road settings is currently affected by a high degree of uncertainty, and more research concerning the strength of VCEs in this type of environment is needed.

The purpose of this article is to investigate the strength of VCEs in an open traffic environment. The study was conducted using CFD calculations with FLACS-CFD v.22.1 [43]. Several scenarios in an open area consisting of groups of vehicles with different configurations were studied. The common setting for all scenarios was a hypothetical accidental release of propane into the atmosphere during transport. This, combined with delayed ignition, resulted in the formation of a vapour cloud on the road which engulfed the group of vehicles. An equivalent cloud with a regular shape and stoichiometric concentration was assumed for all cases. The influence of various geometrical parameters on the resulting overpressure was investigated using the principles of factorial design [44]. The studied parameters included the number of vehicles, the layout of the group of vehicles, the separation distance between vehicles, the gas volume, and the location of the ignition point. Furthermore, the study discussed how the most significant parameters could be used for estimating the strength class as an input for simplified methods, such as the MEM.

This article develops material first presented in Chapter 3 of the main author's licentiate thesis [45] written under the supervision of the coauthors.

2 Methodology

2.1 Overview

The setting of the studied cases was a hypothetical leakage of a flammable gas during transport in an open traffic environment. The fuel gas was assumed to have spread and mixed with the surrounding air to form a vapour cloud that engulfed several vehicles on or near the road. Figure 1 illustrates two examples of such a setting. In Figure 1(a), the gas cloud covers stationary vehicles behind the road tanker from which the flammable gas leaked. In Figure 1(b), the cloud spread outside the road engulfing a group of vehicles parked nearby. The gas cloud eventually ignited, causing a VCE. For the described hypothetical setting, a likely source of strong blast within the cloud is the space between parallel

planes underneath the concentrated group of vehicles [40]. The bodies of the vehicles also provide obstruction to the flow and may contribute to further pressure enhancement.

The approach chosen to conduct the study is illustrated in Figure 2. The work began with the definition of the gas explosion scenarios, including the shape and composition of the gas cloud, the geometry of the mock-up vehicle and the configuration of the group of vehicles. The evaluation of the scenarios relied on numerical simulations based on CFD. The simulation work was carried out in three stages. In the preliminary stage, numerical analyses aimed at finding out the appropriate modelling technique and model parameters were performed. Additionally, a brief study of the influence of the location of the ignition point was conducted to determine suitable ignition locations for the subsequent stage.

The main stage focused on studying the strength of the explosion scenarios. Furthermore, the effect of the scenario parameters on the explosion strength was investigated. The principles of factorial design were employed to perform a cost-efficient parametric study. A comprehensive theoretical background of factorial design can be found in [44]. In conformity with factorial design convention, the term *factor* is used in this article to refer to the parameters that define the explosion scenarios. The investigated influence of the factors included both *main* effects and *interaction* effects. The main effect of a factor is defined as the change in the response (i.e. maximum overpressure) caused by the variation in the level (the term *level* is commonly used to refer to the values that each factor can take) of that factor, averaged over the levels of the other factors. The interaction effects represent the interdependency of effects of two or more factors; that is, the influence of a given factor on the response may change at different levels of the other factors. In a *full* factorial design, all possible combinations of the factors are considered. However, due to the high computational demand of the CFD calculations performed in this study, it was not practical to carry out a full factorial analysis. Instead, two consecutive *fractional* factorial designs were used. In a fractional factorial design, only a carefully selected fraction of the full factorial design is utilised. Initially, a *screening* 2^{6-1} factorial design was implemented (32 scenarios) to identify the factors and interactions with the most significant effects. Six factors, each with two levels, were studied. The most important factors and interactions arising from the screening analysis were then investigated more thoroughly with a *targeted* 3^{4-1} factorial design (27 scenarios), which is a design with four factors, each with three levels.

A necessary step before running the factorial analyses was to choose the range over which the factors would vary. The initial choice was made for the screening 2^{6-1} factorial

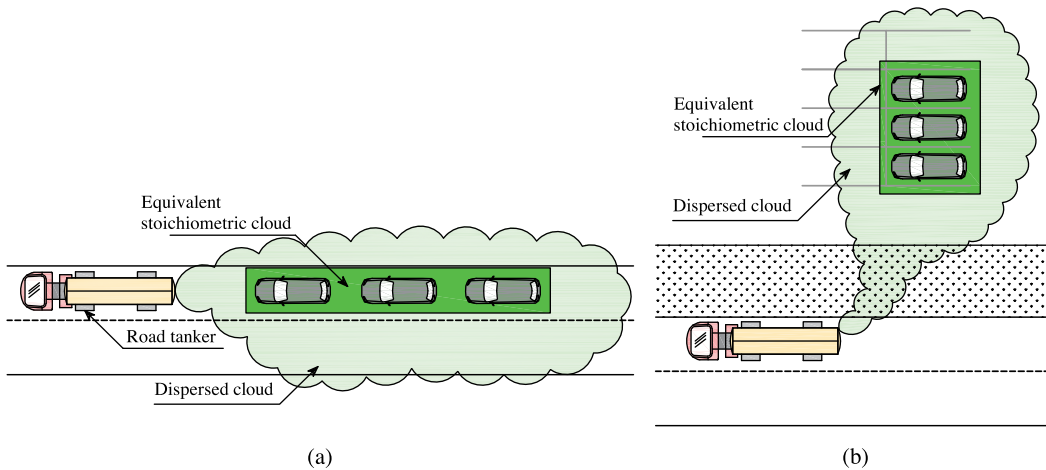


Figure 1: Illustrative examples of scenarios of gas dispersion in a traffic environment relevant for the work in this article: (a) Cloud engulfs vehicles on the road; (b) cloud engulfs vehicles parked near the road.

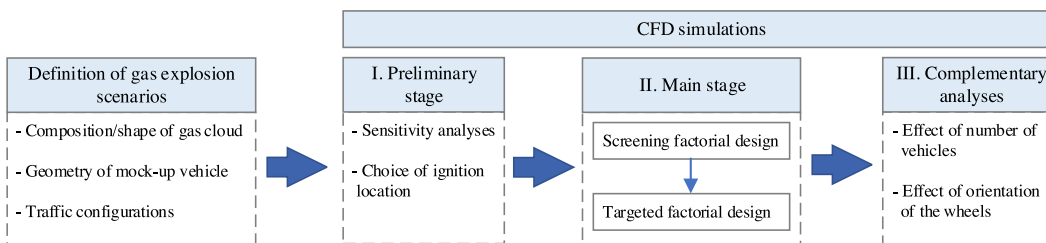


Figure 2: Workflow of the conducted study.

design, in which specific *low* and *high* values were decided for each factor. The choice of levels for the targeted 3^{4-1} design was based on the results from the screening 2^{6-1} factorial design. The terms *low*, *medium*, and *high* are used to refer to the levels of the targeted 3^{4-1} factorial design. The choice of levels is discussed further in Sections 2.3 and 2.4.

Finally, complementary analyses were conducted in the last stage of the study. These analyses focused on the effect of the number of vehicles outside the space of the factorial designs and the influence of the wheels' orientation relative to the main flow direction.

2.2 Scenario definition

In any real traffic situation on an urban road there is normally a broad range of vehicles (e.g. personal cars, trucks, busses, motorcycles), urban furniture (e.g. bus stops, noise barriers, lane dividers, light fixtures), surroundings (e.g. street intersections, carparks, highways, bridge crossings), and environmental conditions (e.g. wind, rain). All these factors may influence both the dispersion and concentration of the gas cloud, as well as

the resulting explosion. However, considering all these factors in a parametric study would require a colossal effort. Therefore, to arrive at a standard case that could lead to useful conclusions with a reasonable amount of resources, several simplifications were implemented.

The most significant simplification in this study concerns the shape and concentration of the vapour cloud. A real dispersed cloud has non-uniform shape and concentration, depending on parameters such as the geometry of the environment and the weather conditions. However, this study modelled the vapour cloud as an equivalent gas cloud shaped as a rectangular cuboid with stoichiometric concentration. The assumption of uniform stoichiometric concentration is meant to represent a worst-case scenario and thus constitutes an upper bound solution regarding the produced overpressure (excluding detonation).

By definition, the equivalent stoichiometric gas cloud (ESC) is expected to produce similar explosion loads as the real dispersed cloud [46, 47]. The volume of the ESC must be smaller than the volume of the real cloud. That is, it was assumed that the volume of the real dispersed cloud was greater than that of the adopted ESC. The largest ESC among the studied scenarios had a volume of around $1,500 \text{ m}^3$. This

volume could be justified by the investigation of the dispersion of the vapour cloud resulting from an unintended release of LPG from a road tanker using CFD by Lozano et al. [48]. Spills in both gaseous and liquid phase with different puncture dimensions were investigated. For each scenario, the volume of the ESC was calculated. Under calm-wind conditions, a release in liquid phase through a puncture with 50 mm diameter was found to lead to ESCs with volume greater than $8,000 \text{ m}^3$. Additionally, releases in gaseous phase were shown to produce ESCs with volume up to 630 m^3 , which is greater than the assumed ESC in many of the scenarios in this article.

The concept of ESC has also been used in other studies to perform consequence analysis of VCEs [8, 32, 49, 50]. Kang et al. [8], in particular, applied CFD to assess the consequences of the accident involving the unintended release of LPG from a road tanker in Wenling, China (2020), which developed into a powerful VCE. A ESC with volume of around $90,000 \text{ m}^3$ was estimated in [8]. With that assumption, the study could effectively replicate the damage range consistent with the real observed damage.

Another simplification involves the type and geometry of the vehicles. All vehicles were assumed to have the same simplified shape, approximately representing a typical personal car in Sweden. The geometry of the vehicle is given in Figure 3(a). The vehicles were arranged in a structured configuration with regular spacing between them. All dimensions were rounded to multiples of 50 mm to ensure a perfect match between the geometry of the vehicle and the

calculation grid. The simplicity of the geometry was also intended to facilitate potential future experimental work.

Six geometrical parameters were chosen to describe the conditions of the analysed scenarios.

- **A**: Separation distance between vehicles.
- **B**: Extension of the gas cloud in the horizontal plane outside the group of vehicles, measured from the perimeter of the group of vehicles.
- **C**: Height of the gas cloud, measured from the ground.
- **D**: Number of vehicles in the transverse direction (y-direction in Figure 3).
- **E**: Number of vehicles in the longitudinal direction (x-direction in Figure 3).
- **F**: Location of the ignition point.

Figure 3(b) shows an example of the gas cloud and the configuration of the group of vehicles for a scenario with 3×3 vehicles. The defining parameters are graphically illustrated in the figure.

The ground clearance (i.e. the distance between the bottom of the vehicle and the ground) is likely to vary within a given group of vehicles. However, treating this property as a variable would significantly increase the number of scenarios and the overall complexity of the study. Thus, a reasonable constant value was desired. A literature study was conducted to support the choice of ground clearance. The experimental research described in [12, 30] adopted a ground clearance of 300 mm. Middha and Hansen [27] assumed values of ground clearance of 200 mm and 300 mm

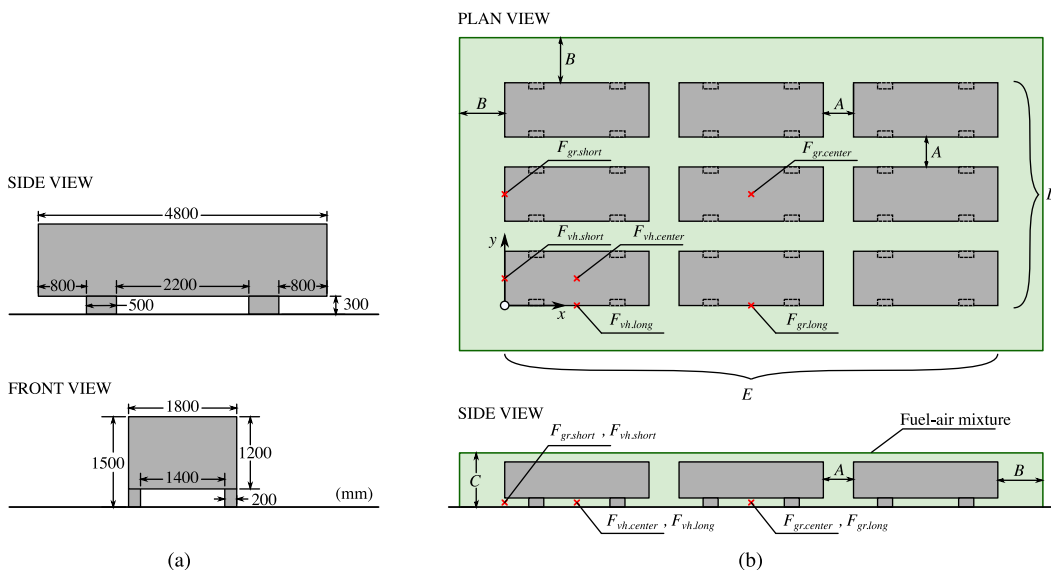


Figure 3: Schematic representation of the gas cloud and configuration of the vehicle group: (a) geometry of mock-up vehicle; (b) parameters defining the gas explosion scenarios. The ignition point, marked with a red cross, is placed at 0.175 m above ground.

for personal vehicles and 400 mm for busses to investigate the risk associated with hydrogen vehicles in tunnels. In [51], a ground clearance of 150 mm was assumed for personal vehicles to conduct a risk analysis of LPG vehicles in enclosed car parks. Lozano et al. [52] investigated the effect of varying the ground clearance between 150 and 500 mm on the resulting overpressure. For the scenarios analysed in that study, it was concluded that using 300 mm produced overpressure values that approximated the average overpressure across all the studied values of ground clearance. Based on the literature review, a ground clearance of 300 mm was adopted for all scenarios in this study.

Different scenarios were generated by varying the defining parameters shown in Figure 3(b). 32 scenarios were used in the screening 2^{6-1} factorial design, and 27 were used in the targeted 3^{4-1} factorial design (six scenarios appeared in both factorial designs).

The study assumed that the gas cloud consisted of a mixture of propane and air. The main reason for this choice is that LPG is the most frequently transported fuel gas in Sweden, and often forms the basis for risk analysis related to transport of flammable gases in the country [53, 54]. LPG mixes sold in Sweden typically consist of at least 95 % propane, along with other hydrocarbon gases such as butane [55]. Since the reactivity of butane is similar to that of propane, a stoichiometric mixture of propane and air was chosen for all cases.

2.3 Screening 2^{6-1} factorial design

The main stage of this study started with a screening analysis using a 2^{6-1} factorial design. This is a resolution VI design, in which the main effects are confounded with five-factor interactions, and the two-factor interactions are confounded with four-factor interactions [44]. The four-factor and higher-order interactions are likely negligible, making this design suitable for studying all main effects and two-factor interactions.

The low and high values chosen for each factor are summarised in Table 1. The low value of factor A (separation distance between vehicles) was set to 0.5 m, representing the distance between tightly parked vehicles. The high value was set to 1.5 m, which approximately represents the distance between personal vehicles centred in their respective lanes on a typical road in Sweden. The low and high values for factor B were set to 0.0 m and 4.0 m, respectively. The low value corresponds to a scenario in which the gas cloud occupies the same area (in the horizontal plane) as the group of vehicles. The high value was chosen to be slightly greater than twice the width of the vehicles. The low value of factor C

(gas cloud height) was set to 1.8 m. This value corresponds to the recommended height of the congested volume due to a group of vehicles in a carpark given in [56]. The high value was set to twice the low value.

Factors D and E (the number of vehicles in the transverse and longitudinal direction) are both discrete. Their low value was set to 1, while the high value was set to 3. Situations in which the number of vehicles exceeds 3 are common. For example, a row of cars parked side by side outside a shopping centre could have more than 3 cars. Similarly, queues of vehicles at traffic lights often extend beyond 3 vehicles. In these situations, D and E could potentially become greater than 3 provided that the gas volume is large enough and the concentration of the fuel-air mixture is within the flammability limits. However, the choice of the high value was constrained by the high computational demand of the CFD calculations, as more vehicles would increase the size of the calculation domain. Nonetheless, a high value equal to 3 was deemed reasonable and should enable observation of the effects of these factors.

Deciding on a low and high level for the location of the ignition point (factor F) was more challenging due to its multidimensional nature. Before performing the calculations required for the factorial designs, a preliminary study was conducted to assess the influence of the location of the ignition point. This preliminary study focused on a single configuration consisting of nine vehicles in a 3×3 layout, with an equivalent stoichiometric propane-air cloud with dimensions $19.4 \times 10.4 \times 1.8$ m ($A = 0.5$ m, $B = 2.0$ m, $C = 1.8$ m, $D = E = 3$). Six ignition point locations were tested, as shown in Figure 3(b). The results and conclusions from this preliminary study are presented in Section 4.1. Based on the results, locations $F_{\text{vh.short}}$ and $F_{\text{gr.long}}$ were adopted as the low and high level.

Table 2 shows the different combinations for the screening 2^{6-1} factorial design along with the maximum overpressure, P_{max} , obtained for each scenario (discussed in Section 4.3). The levels of factor F were calculated with the design generator $F = ABCDE$.

2.4 Targeted 3^{4-1} factorial design

According to the results presented in Section 4.3, the most significant effects that emerged from the screening design were the main effects of A , C , B and D along with the interaction effects AD , BD , and CD . A more detailed investigation of the influence of these factors on the maximum overpressure was conducted using a 3^{4-1} fractional factorial design. Note that several 3^{4-1} designs can be derived from a full 3^4 factorial design. The design used here was specifically

Table 1: Factors and levels used in the factorial designs.

Factor	Description	Screening analysis		Targeted analysis			Unit
		Low (–)	High (+)	Low (0)	Medium (1)	High (2)	
A	Distance between vehicles	0.5	1.5	0.5	1.5	2.5	m
B	Extension of the cloud in the horizontal plane beyond the group of vehicles	0.0	4.0	0.0	2.0	4.0	m
C	Height of the cloud	1.8	3.6	1.8	2.7	3.6	m
D	Number of vehicles in the transverse direction	1	3	1	2	3	–
E	Number of vehicles in the longitudinal direction	1	3	3			–
F	Location of the ignition point	$F_{\text{vh,short}}$	$F_{\text{gr,long}}$	$F_{\text{gr,long}}$			–

Table 2: Scenarios in the screening 2^{6-1} factorial design. The symbols “–” and “+” represent the low and high level according to Table 1. P_{max} is the maximum overpressure obtained from the CFD calculations.

Scenario	A	B	C	D	E	F	P_{max} (kPa)
1-01	–	–	–	–	–	–	2
1-02	–	–	–	+	–	+	8
1-03	–	–	–	–	+	+	3
1-04	–	–	–	+	+	–	7
1-05	–	–	+	–	–	+	2
1-06	–	–	+	+	–	–	10
1-07	–	–	+	–	+	–	3
1-08	–	–	+	+	+	+	25
1-09	–	+	–	–	–	+	7
1-10	–	+	–	+	–	–	17
1-11	–	+	–	–	+	–	5
1-12	–	+	–	+	+	+	27
1-13	–	+	+	–	–	–	16
1-14	–	+	+	+	–	+	39
1-15	–	+	+	–	+	+	16
1-16	–	+	+	+	+	–	44
1-17	+	–	–	–	–	+	2
1-18	+	–	–	+	–	–	11
1-19	+	–	–	–	+	–	4
1-20	+	–	–	+	+	+	36
1-21	+	–	+	–	–	–	3
1-22	+	–	+	+	–	+	41
1-23	+	–	+	–	+	+	4
1-24	+	–	+	+	+	–	22
1-25	+	+	–	–	–	–	8
1-26	+	+	–	+	–	+	43
1-27	+	+	–	–	+	+	9
1-28	+	+	–	+	+	–	32
1-29	+	+	+	–	–	+	9
1-30	+	+	+	+	–	–	77
1-31	+	+	+	–	+	–	21
1-32	+	+	+	+	+	+	106

chosen to ensure that no main effect is confounded with any two-factor interaction. Moreover, the three more significant interactions from the initial 2^{6-1} design (AD , BD , and CD) are

free from confounding with any other two-factor interaction. Assuming that the three-order and four-order interactions are negligible, this design is suitable for evaluating the main effects and the three most relevant two-factor interactions. However, the remaining two-factor interactions are confounded with other two-factor interaction components. Separating the effects of these remaining two-factor interactions was not attempted in this work.

The low, medium, and high levels used in the 3^{4-1} factorial design are summarised in Table 1. The medium values for factors B , C , and D were calculated as the average of their respective low and high values used in the screening analysis. For factor A , the centre point was set to 1.5 m, while the high value was set to 2.5 m. Factors E and F were set to their high level. Table 3 gives the different combinations for this design and the maximum overpressure, P_{max} , for each scenario (discussed in Section 4.4).

3 CFD modelling

3.1 Brief description of FLACS-CFD

FLACS-CFD [43] is a finite volume code designed to solve the Navier–Stokes equations of compressive flow, along with combustion and turbulence, on a structured cartesian grid. A comprehensive description of the theoretical background of FLACS-CFD is given in [57–59].

Calculations in FLACS-CFD rely on the Porosity Distributed Resistance (PDR) approach [60, 61] in combination with several sub-grid models to account for the effects of sub-grid objects on turbulence generation and flame wrinkling. Turbulence is modelled with the standard k - ϵ turbulence model [62]. The combustion model consists of three main parts: a numerical flame model, a burning velocity model, and a flame-folding model. The numerical flame model, based on the work in [59], artificially thickens the flame zone

Table 3: Scenarios in the targeted 3^{4-1} factorial design. The digits “0”, “1” and “2” represent the low, medium, and high level according to Table 1. P_{\max} is the maximum overpressure obtained from the CFD calculations.

Scenario	A	B	C	D	P_{\max} (kPa)
2-01	0	0	0	0	3
2-02	0	0	1	1	12
2-03	0	0	2	2	25
2-04	0	1	0	1	16
2-05	0	1	1	2	45
2-06	0	1	2	0	11
2-07	0	2	0	2	27
2-08	0	2	1	0	10
2-09	0	2	2	1	31
2-10	1	0	0	1	14
2-11	1	0	1	2	66
2-12	1	0	2	0	4
2-13	1	1	0	2	48
2-14	1	1	1	0	12
2-15	1	1	2	1	45
2-16	1	2	0	0	9
2-17	1	2	1	1	43
2-18	1	2	2	2	106
2-19	2	0	0	2	27
2-20	2	0	1	0	5
2-21	2	0	2	1	29
2-22	2	1	0	0	8
2-23	2	1	1	1	32
2-24	2	1	2	2	66
2-25	2	2	0	1	19
2-26	2	2	1	2	58
2-27	2	2	2	0	16

by increasing the diffusion with a factor β , and decreasing the reaction rate with a factor $1/\beta$. It was designed to ensure that the numerical flame zone propagates with the specified burning velocity. The burning velocity model implements a series of empirical correlations that link the burning velocity to the properties of the mixture and the flow regime (i.e. laminar, quasi-laminar, or turbulent flow). Finally, the enhancement in burning rate due to folding of the flame around the sub-grid obstacles and some hydrodynamic instabilities is handled by the flame-folding model.

3.2 Modelling approach

The calculation domain was divided into a *core domain* (from which results are gathered) and a *stretched domain* (buffer zone between the core domain and the boundary conditions). Cubical cells with a size of 50 mm were used within the core domain. Outside the core domain, the cell size was gradually stretched using a geometrical progression

with a factor of 1.2. Table 4 gives the values of relevant model parameters adopted in this study. The choice of cell size is discussed in Section 3.3. Non-reflecting boundary conditions (known as PLANE_WAVE) were applied at all outlets. The ground was modelled as a rigid surface. The mock-up vehicles and undisturbed unburned vapour cloud were placed entirely within the core domain. Care was taken to align the edges of the geometry of the vehicles with the grid. Thus, the porosity values in the studied scenarios were either 0 (completely blocked cell) or 1 (completely open cell). Lastly, the option STEP = “KEEP_LOW” was used to ensure sufficiently short time steps in the later stages of the simulation to prevent artificial numerical damping of the pressure waves.

In general, the core domain was defined by $x = [-4 \text{ m}, 30 \text{ m}]$, $y = [-4 \text{ m}, 20 \text{ m}]$ and $z = [0 \text{ m}, 8 \text{ m}]$, although larger core domains were used in the largest scenarios. Ideally, the core domain should be large enough so that combustion occurs entirely within this domain. However, this would result in an unreasonably large number of cells with the chosen grid cell size. Since only results in the positive quadrant were of interest (Figure 3(b) shows the location of the origin), the core domain was extended sufficiently in the *positive* x - and y -direction to ensure that the flame front never left the domain in those directions. However, the extension of the core domain towards the *negative* x - and y -direction was limited to reduce the computational demand. Consequently, the flame front travelled into the stretched domain in the negative x - and y -direction at some point during the simulation. The effect of the flame’s propagating into the stretched domain in the negative directions was investigated in a few cases and found to have little impact on the results in the region of interest. The dimensions of the entire calculation domain varied between approximately $60 \times 60 \times 12 \text{ m}$ (around 55×10^6 cells) for the scenarios with the smallest gas volume and about $90 \times 90 \times 16 \text{ m}$ (around 75×10^6 cells) for the scenarios with the largest gas volume. A picture of a sample model appears in Figure 4. The simulations were carried out in parallel using 16 CPUs.

Table 4: Relevant model parameters adopted in the CFD simulations.

Model parameter	Value
Characteristic velocity	10 m/s
Relative turbulence intensity	0.1
Turbulence length scale	50 % of the cell size
Courant-Friedrich-Levy number based on sound velocity, CFLC	5 (default value)
Courant-Friedrich-Levy number based on flow velocity, CFLV	0.5 (default value)

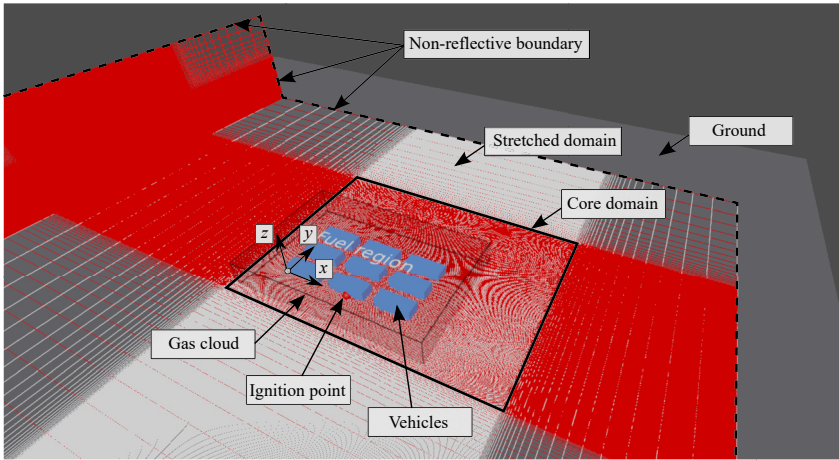


Figure 4: Example of a model with 3×3 vehicles (scenario 1–32).

3.3 Choice of grid cell size

The user's manual for FLACS-CFD [43] specifies a maximum grid cell size for gas explosion simulations defined as $L_{\text{cloud.min}}/15$, in which $L_{\text{cloud.min}}$ is the smallest extent of the flammable cloud. Thus, for the smallest cloud height in this study (1.8 m), the maximum grid cell becomes 120 mm. Additionally, the minimum allowed grid cell size according to the user's manual is 10 mm. Besides these restrictions, the chosen grid cell size should ensure proper results in the region between the vehicles and the ground. The reason for this is that combustion and expansion underneath the group of vehicles, where the flow is largely two-dimensional, is believed to have an important effect on the resulting explosion.

Lozano [63] conducted a grid sensitivity and validation study of simulations of fuel-air mixture explosions in a traffic environment using FLACS-CFD. The overall aim of that study was to give recommendations for the choice of grid cell size based on comparison between gas explosion experiments and corresponding FLACS-CFD simulations with different grid resolutions and varying modelling parameters. Lozano [63] based the recommendations on two gas explosion experiments consisting of obstructed two-dimensional setups, representative of the conditions underneath a concentrated group of vehicles. The first experiment studied was the large-scale experiment by van Wingerden [64], which investigated the deflagration of ethylene-air mixtures in a congested region confined between two planes with obstacles in the form of parallel horizontal tubes (101.6 mm diameter and 3.0 m length). The area of the top confining plate was $4 \text{ m} \times 4 \text{ m}$. Different values of the distance between the confining planes, h , were used. The second experiment studied was reported by van Wingerden [65]. That experiment also investigated deflagration between two parallel planes, but with obstacles

arranged as concentric semi-circles of vertical tubes (80 mm diameter). Three different gases were investigated: methane, propane and ethylene. The area of the top confining plate was $4 \text{ m} \times 2 \text{ m}$. A wall of symmetry was placed along the long side of the configuration. The distance between the confining planes was 160 mm. Lozano [63] adopted the first experiment [64] as the basis for the choice of grid cell size, while the second experiment [65] was used to test the conclusions reached from the analysis of the first experiment.

The analysis of the first experiment [64] showed that acceptable predictions could be obtained if the main direction of confinement, h , is discretised with three to six cubic grid cells. This is clear in Figure 5, which compares the experimental flame speed inside the congested region with the results from simulations with different cell counts,

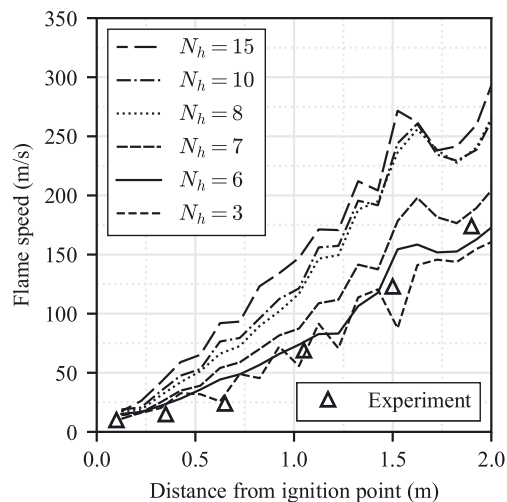


Figure 5: Comparison of the experiment in [64] with FLACS-CFD simulations, as reported in [63]: Flame speed versus distance for different values of cell count, N_h . The distance between confining planes was $h = 300 \text{ mm}$. The grid cell size is calculated as h/N_h .

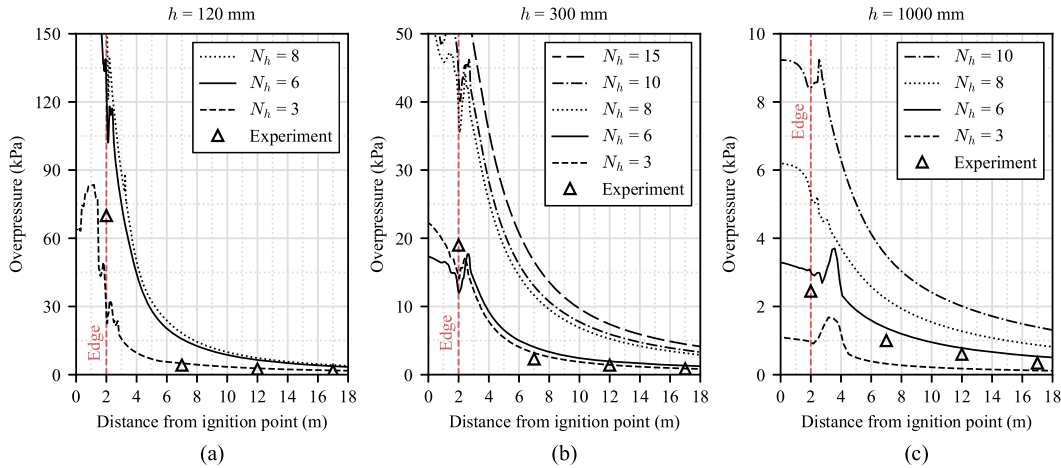


Figure 6: Comparison of the experiment in [64] with FLACS-CFD simulations, as reported in [63]: Peak overpressure versus distance for different values of cell count, N_h , and the distance between confining planes, h . The grid cell size is calculated as h/N_h .

N_h , between confining planes in a configuration with $h = 300$ mm. For a given N_h , the corresponding grid cell size (h/N_h) was used throughout the entire numerical model.

Similarly, discretizing the main direction of confining into three to six cells produced acceptable prediction of peak overpressure outside the congested region, as evidenced in Figure 6. These results indicate that choosing a cell count between $N_h = 3$ and $N_h = 6$ would lead to reasonable results both inside and outside the confined region. This range of cell count was also used by Middha [66] to simulate hydrogen explosions in a vehicle refuelling environment. Greater values of N_h (i.e. a smaller grid cell size) would lead to overly conservative results. Moreover, these conclusions seemed to hold for different values of the distance between confining planes.

Similar conclusions were drawn from the comparison between the second experiment [65] and FLACS-CFD simulations. Figure 7 shows the comparison between the measured and predicted flame speed for a configuration with $h = 160$ mm and a mixture of propane and air. The results confirmed that the models discretised based on $N_h = 3$ and $N_h = 6$ provided a reasonable lower and upper bound of the prediction.

Based on these results presented in [63], a cell count of $N_h = 6$ was chosen to discretize the ground clearance. This choice may lead to some degree of overprediction of the overpressure generated by the explosion. However, the overprediction, if any, is expected to be within the same order of magnitude. Middha [66] has also previously reasoned that using six grid cells for resolving the flow in the space underneath a vehicle is more optimal than using three cells, which is consistent with the choice made here. Thus, for the ground clearance adopted in this study (300 mm), the

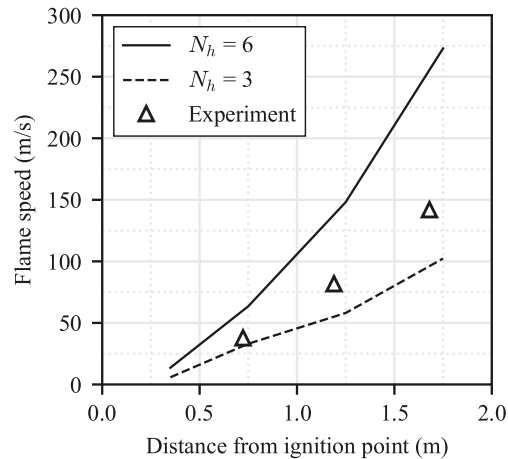


Figure 7: Comparison of the experiment in [65] (propane-air mixture) with FLACS-CFD simulations, as reported in [63]: Flame speed versus distance for different values of cell count, N_h . The distance between confining plane was $h = 160$ mm. The grid cell size is calculated as h/N_h .

grid cell size within the core domain was calculated as $300 \text{ mm}/6 = 50 \text{ mm}$. This grid cell size is within the allowed interval ($10 \text{ mm} < 50 \text{ mm} < 120 \text{ mm}$).

4 Results and discussion

4.1 Location of the ignition point

As outlined in Section 2.3, a preliminary study of the influence of the location of the ignition point was conducted to identify suitable low and high levels for this parameter. The results of these calculations are presented in Figure 8 as contour plots of peak overpressure. At each point (x, y) , the

plots show the greatest overpressure obtained along the z -direction. P_{max} is the maximum overpressure obtained within the region of interest: $x = [0 \text{ m}, 30 \text{ m}]$, $y = [0 \text{ m}, 20 \text{ m}]$ and $z = [0 \text{ m}, 8 \text{ m}]$. P_{mean} refers to the *mean* peak overpressure within the bounding box of the group of vehicles.

The initial observation is that centre ignition (scenario 0–02) did not result in the most severe explosion. Greater

values of maximum overpressure were observed in the cases in which the ignition point was located at or near the long edge of the group (scenarios 0–01, 0–03 and 0–04). However, centre ignition did not result in the weakest explosion either. Indeed, the cases with ignition at the short edge of the group were the least severe (scenarios 0–05 and 0–06). This suggests that a longer propagation distance alone

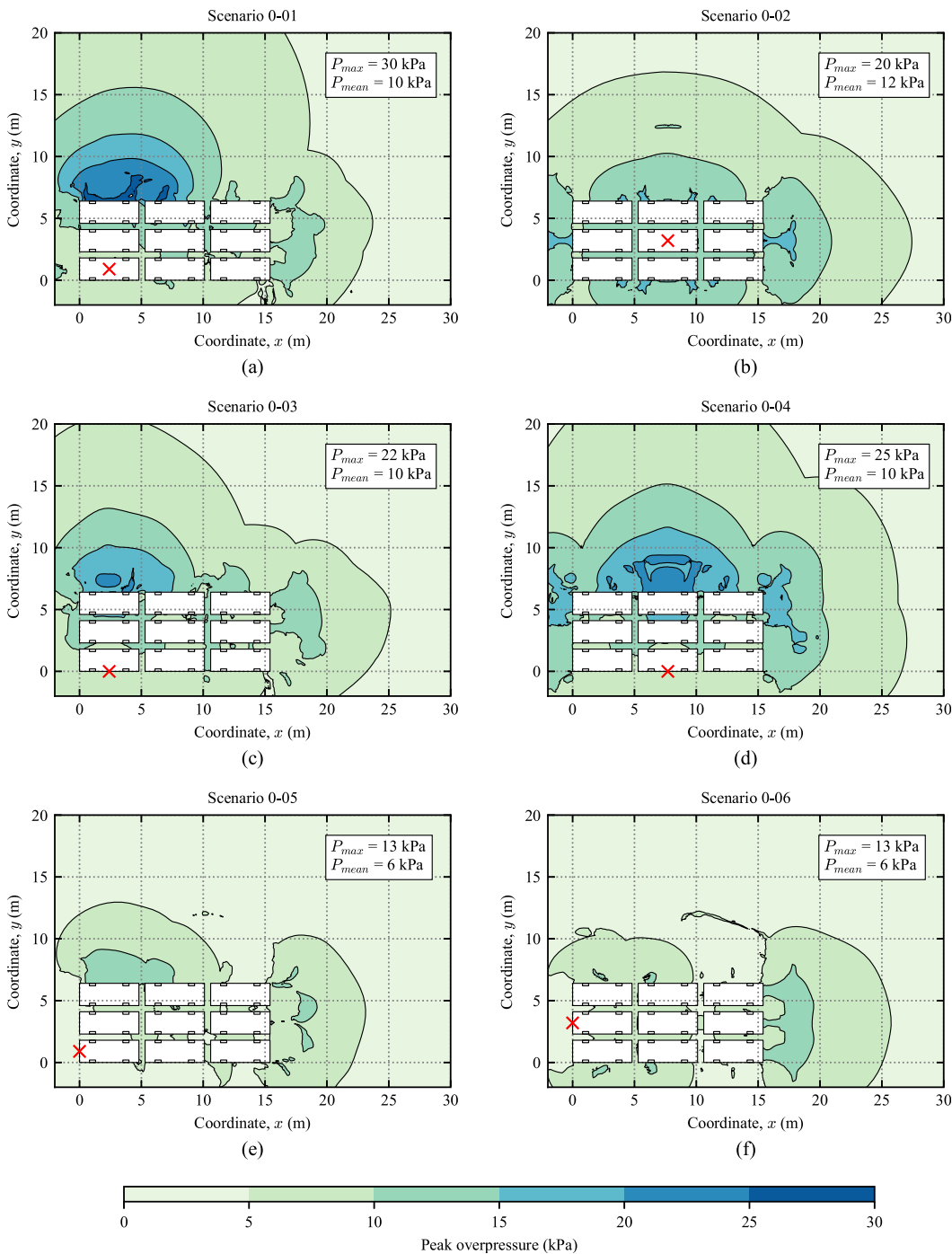


Figure 8: Contour plot of peak overpressure for different locations of the ignition point. The red cross gives the location of the ignition point.

might not be sufficient to enable pressure build-up. Instead, it appears that it is the combined influence of the distance covered by the flame and the shape of the obstacles in the confined region (wheels) that may prevail over the calming effect of side relief. An interesting observation is that, while centre ignition did not yield the greatest P_{\max} , it did produce the greatest value of mean peak overpressure, P_{mean} , within the congested region.

Based on these results, the ignition point at the short edge of the corner vehicle, $F_{\text{vh.short}}$, was selected as the low level. Conversely, edge ignition at the middle of the long edge of the group of vehicles, $F_{\text{gr.long}}$, was chosen as the high level. Although $F_{\text{gr.long}}$ did not produce the greatest value of maximum overpressure, this location was chosen because it appears to allow for a larger amount of combustion energy to contribute to strong blast generation based on the profile of peak overpressure outside the vehicle cluster.

4.2 General evaluation of the results

Before delving into the results concerning the factorial designs, it is of interest to examine the distribution of maximum overpressure values obtained from the evaluated scenarios. Figure 9 gives this distribution, with the values grouped into six intervals. The lowest maximum overpressure was 2 kPa (scenario 1–17). Conversely, the greatest value of maximum overpressure was 106 kPa (scenario 1–32). Approximately 90 % of all scenarios produced a maximum overpressure that was less than 50 kPa. That is, overpressure values greater than 50 kPa occurred only in a few cases with the most unfavourable conditions considered here. It should be noted that these values of maximum overpressure were calculated on congested regions fully immersed in a stoichiometric propane-air cloud. Thus, these values are meant to represent a worst-case scenario. Lower values may be obtained in scenarios that are geometrically identical, but with flammable clouds with non-uniform concentration and arbitrary shape.

It is also pertinent to assess the characteristics of the resulting explosion for a few selected cases to evaluate the validity of the results and draw some general conclusions. This assessment was carried out for four different scenarios: 1–26, 1–27, 1–29 and 1–32. The selected cases share the following parameters: $A = 1.5$ m, $B = 4$ m, and $F = F_{\text{gr.long}}$. Contour plots of peak overpressure for these scenarios are shown in Figure 10. At each point (x, y) , the contour plots display the greatest overpressure obtained along the z -direction.

The case with a single vehicle (scenario 1–29) exhibited a nearly radial and symmetric distribution of peak

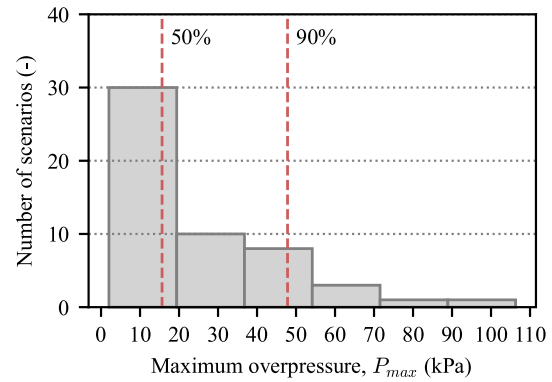


Figure 9: Distribution of maximum overpressure for the studied scenarios.

overpressure around the vehicle, despite the edge ignition. This suggests that this case could be regarded as a single explosion in terms of blast generation.

In the scenarios with three vehicles in the y -direction (scenarios 1–26 and 1–32), the peak overpressure contours were clearly asymmetric with a strong degree of directionality. The greatest overpressure values occurred in a localised area on the opposite side of the group of vehicles relative to the ignition point. This was likely the result of flame acceleration as it travelled through the congested region, combined with pressure build-up when the flame front entered the turbulent recirculation zone past the group of vehicles. Indeed, large values of overpressure in the region behind a vehicle due to a gas deflagration have been previously experimentally observed in [30]. Moreover, it appears that the energy contributing to the maximum overpressure was relatively limited in comparison with the total gas inventory, based on the limited radius of influence of the zone with large overpressure values. This suggests that, for estimating the blast load in the vicinity of the explosion, the localised areas with large values of overpressure could potentially be regarded as independent stronger localised explosions with a small effective volume of flammable mixture. Combustion of the remaining (and greater) gas volume would describe the overall explosion, which would be characterised by a lower strength.

The contour plot for scenario 1–27 showed a relatively small degree of asymmetry. In this scenario, there was no clear localised area with significantly higher overpressure, as it was the case in scenarios 1–26 and 1–32. In other words, this scenario could be treated as a single explosion in terms of blast generation. Notably, the presence of more vehicles in this scenario did not result in greater strength compared to scenario 1–29. Instead, both cases displayed an explosion strength of around 9 kPa. However, it appears that the amount of energy contributing to blast generation was

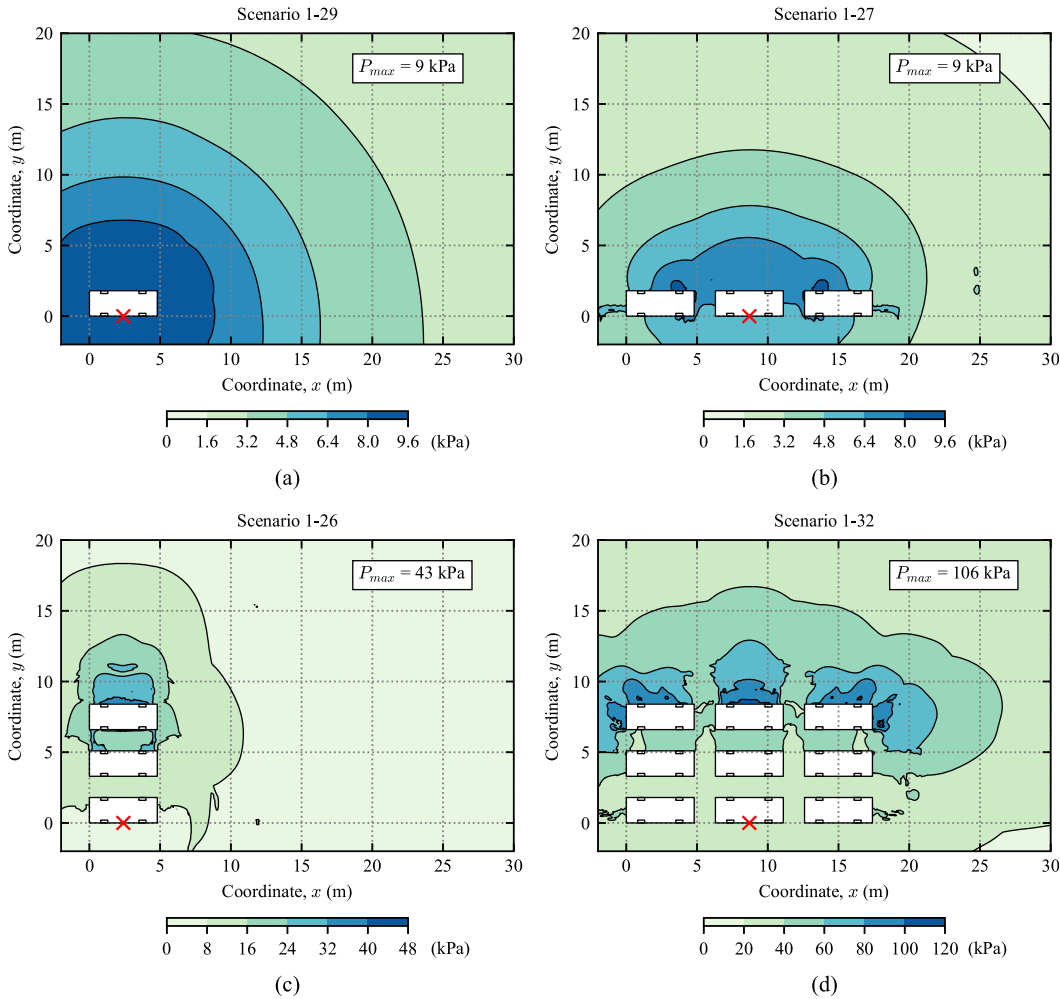


Figure 10: Contour plots of peak overpressure for selected scenarios. The red cross gives the location of the ignition point.

greater in scenario 1–29, as the decay of pressure occurred over a longer distance in this scenario. The total gas volume was only slightly larger for scenario 1–29 (441 m^3 for 1–29 and 417 m^3 for 1–27), which indicates that the greater amount of energy in scenario 1–29 was not due to a larger gas volume, but more likely due to the shape of the gas cloud.

Overpressure-time histories at different monitor points for two selected scenarios are shown in Figure 11. The monitor points were located on a path along the y -direction at $x = 2.0 \text{ m}$ in scenario 1–29 and at $x = 8.0 \text{ m}$ in scenario 1–32. The overpressure-time curves for the weaker explosion (scenario 1–29) could be described as sonic waves in which the pressure increases gradually followed by a gradual drop in pressure. In this scenario, the amplitude of the negative phase was similar to that of the positive phase. This phenomenon has also been highlighted by other researchers, see e.g. [36]. Conversely, the stronger explosion (scenario 1–32) showed a more rapid increase of pressure, making it more similar to a shock wave. Furthermore, the overpressure-time

history for the stronger explosion had several smaller peaks, whereas less noise was observed for the weaker explosion. For the stronger explosion, the peak overpressure in the positive phase clearly decreased as the distance to the studied point increased. However, the amplitude of the pulse in the negative phase was similar regardless of the distance.

Curves of peak overpressure as a function of distance are presented in Figure 12. The results were taken along the same paths on which the monitor points in Figure 11 were located. For scenario 1–29, it can be observed that the peak overpressure remained almost constant for some meters beyond the congested region before pressure decay began. This could indicate that the effects of confinement and turbulence within the congested region were not significant in this scenario, so that the flame continued to burn with a similar regime outside the congested region, maintaining the pressure values. In contrast, a sharp and discrete increase of pressure was observed immediately outside the congested region for scenario 1–32. Potential reasons for this

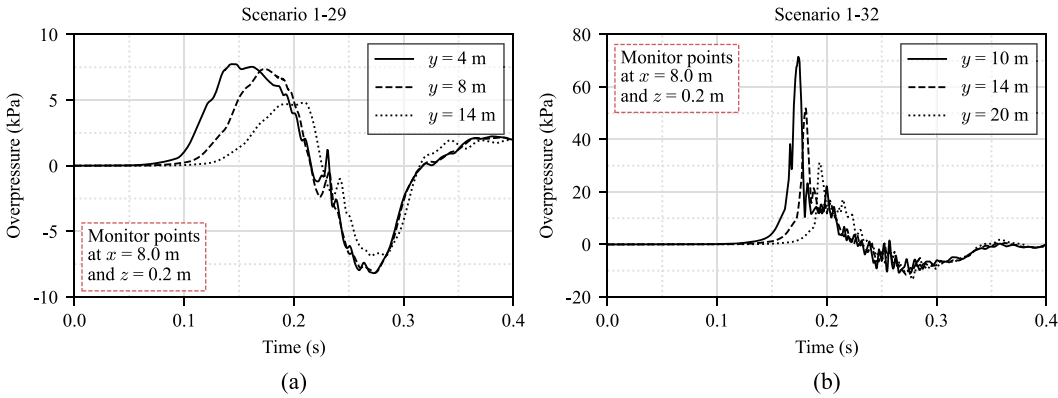


Figure 11: Overpressure-time curves for two selected scenarios at selected monitor points. See also Figure 12.

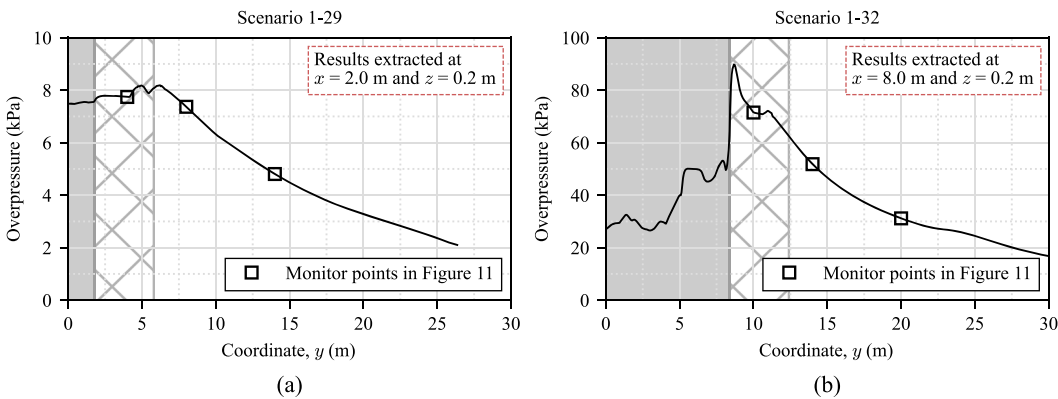


Figure 12: Overpressure-distance curves at selected paths. The shaded area represents the region occupied by the vehicles. The hatched area represents the undisturbed unburned gas outside the group of vehicles. The squares represent the monitor points in Figure 11.

include reflection against the vehicle and high turbulence just outside the congested region. In this case, decay of pressure occurred immediately after the position of maximum overpressure. This may indicate that combustion outside the group of vehicles evolves in a markedly different regime compared to combustion through the congestion region.

4.3 Screening 2^{6-1} factorial design

The maximum overpressure, P_{\max} , obtained for each scenario in the screening 2^{6-1} design is given in Table 2. The main effects are plotted in Figure 13. The main effect of a factor is defined as the change in maximum overpressure caused by the variation in the level of the factor, averaged over the levels of all other factors. All main effects were positive, meaning that increasing the value of a given factor is likely to lead to an increase in maximum overpressure, if there are no significant negative interaction effects involving that factor.

Figure 14 displays the estimates of the main and two-factor interaction effects ordered by magnitude. The estimate of the main effect in Figure 14 was calculated as the difference between the average overpressure at the two levels of the factor (compare with Figure 13). The only negative effect was the interaction BF . However, this interaction was found negligible compared to the other effects.

The most significant main effects identified by this analysis were the effects of A , B , C , and D . The number of vehicles in the transverse direction (factor D) had the greatest influence on the maximum overpressure, followed by the extension of the cloud (factor B), the height of the cloud (factor C), and the separation distance between vehicles (factor A). On the other hand, factor E (number of vehicles in the longitudinal direction) had the least significant influence on the response. Finally, the location of the ignition point (factor F) appeared to have a minor influence compared to factors A to D . This indicates that E and F do not need to be included in the following phase of the study.

Figure 14 shows that some two-factor interactions are also significant. The interactions between factor D and the

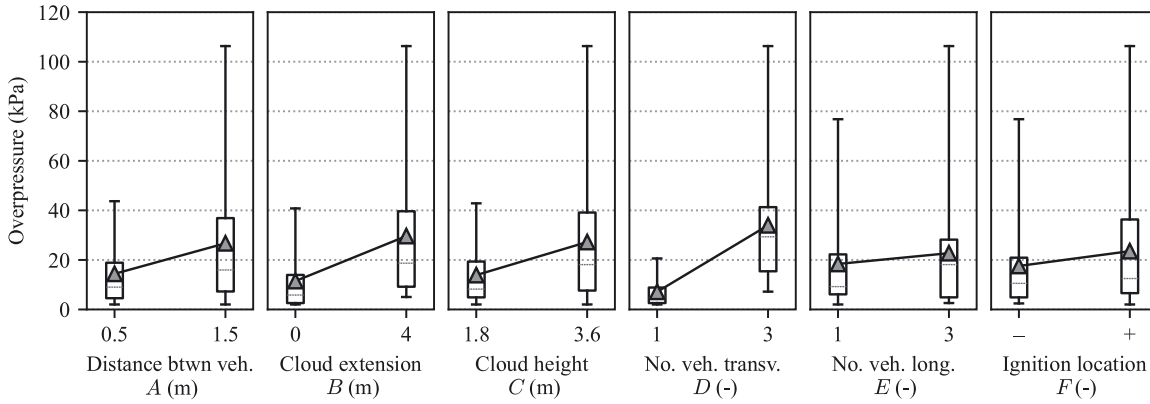


Figure 13: Main effects of the independent factors obtained from the screening 2^{6-1} fractional factorial design. The boxes extend from the 25th to the 75th percentile. The triangles represent the mean value.

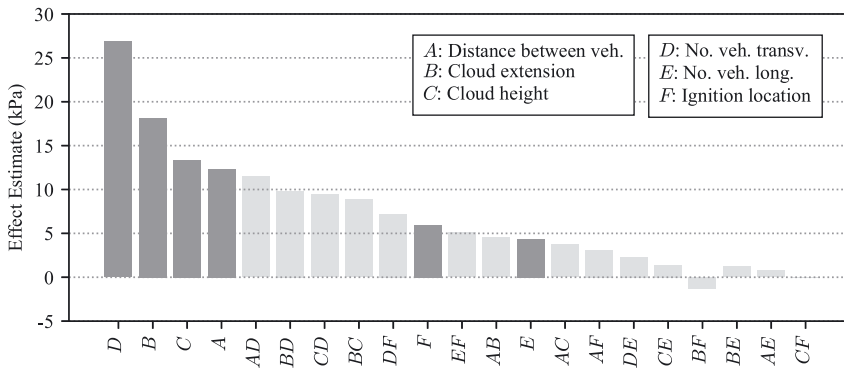


Figure 14: Estimates of main effects (dark grey) and two-factor interaction effects (light grey) obtained from the screening 2^{6-1} fractional factorial design.

three other most relevant parameters (AD , BD , CD) emerged as the most relevant interactions. The interaction effects BC and DF also had a noticeable effect, even greater than the main effects of E and F . The most important interactions effects are plotted in Figure 15. In plots of interaction effects, if the interaction between two factors were negligible, the corresponding lines would be nearly parallel. The effect of factors A , B , and C were found to be small when D takes its

low value ($D = -$). These effects significantly increased when $D = +$. A similar situation could be discerned for the interaction effect EF ; that is, the effect of E was nearly null for $F = -$, but it increased when $F = +$.

The contrast between the main effects of the number of vehicles in the transverse direction, D , and the number of vehicles in the longitudinal direction, E , was an interesting finding. While D had the most significant effect on the

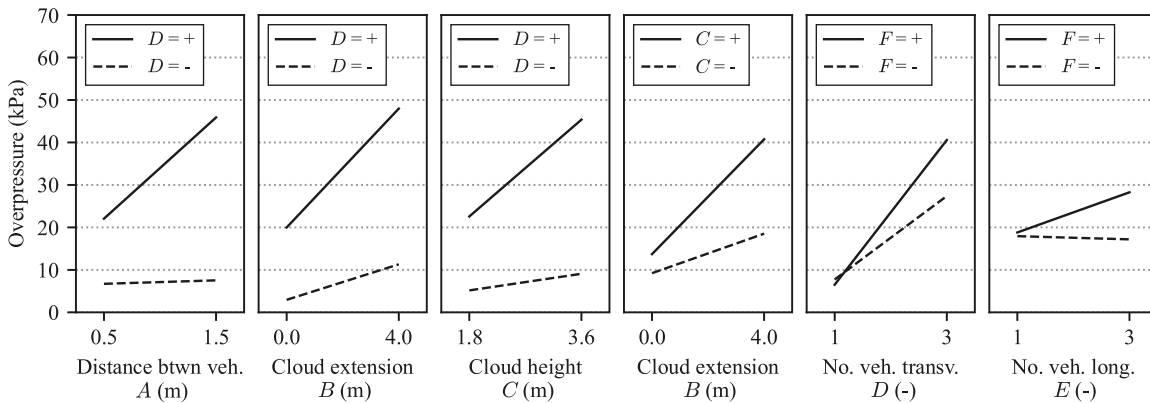


Figure 15: Most significant two-factor interaction effects obtained from the screening 2^{6-1} fractional factorial design.

overpressure, factor E had the least significant effect. This suggests that, regarding the strength of a VCE on a road, the number of lanes plays a much more important role than the length of the traffic queue. Furthermore, there is a greater potential for powerful accidental explosions in carparks where vehicles park side by side.

It is believed that the difference between the effects of factors D and E was caused by a relatively strong influence of the interaction of the flow with the obstacles under the vehicles (i.e. wheels). While factor D relates to the distance that the flame travels perpendicularly to the wheels (i.e. the flame front meets the “long” side of the wheels), factor E is related to flame travel distance parallel to the wheels (i.e. the flame front meets the “short” side of the wheels). That is, the greater effect of D compared to the effect of E may be related to more intense turbulence generation caused by the interaction of the flow with the “long” side of the wheel. This topic is treated in more detail in Section 4.5.2.

Considering the low significance of the main effect of E and the interaction DE for the range studied here, two tentative conclusions could be drawn. First, a case with $D > 3$ and $E = 3$ will produce greater overpressure values than an equivalent case with $D = 3$ and $E = 3$. Moreover, the overpressure might continue to increase for larger values of D . Second, a case with $D = 3$ and $E > 3$ will yield similar overpressure values to those from a case with $D = 3$ and $E = 3$. To confirm these conclusions, it is necessary to evaluate scenarios with more vehicles than those considered in the factorial designs. This topic is addressed in Section 4.5.1.

4.4 Targeted 3^{4-1} factorial design

The maximum overpressure values, P_{\max} , obtained for each scenario in the targeted 3^{4-1} factorial design are summarised in Table 3. The significance of the different effects was investigated with the analysis of variance (ANOVA) in Table 5. The ANOVA is generally employed to identify factors

within a factorial design that are likely to be important [44]. The effects were arranged in ascending order of P -value. A small P -value indicates strong statistical evidence against the null hypothesis (that there is no significant relationship between the factor and the resulting overpressure). To estimate the error in the ANOVA, the remaining two-factor interactions and all higher-order interactions were assumed to be negligible. The last column in the table shows the contribution to the variation based on the sum of squares. The main effects from the 3^{4-1} factorial design are plotted in Figure 16.

The ANOVA confirmed that the main effect of D dominates the variation of overpressure (P -value < 0.001), accounting for over 50 % of the total variability. Figure 16 also shows a strong positive effect of factor D on the explosion strength: an increase of D consistently led to a significant increase in maximum overpressure. Moreover, the average change in response due to the variation of this factor appears to be nearly linear. Given the importance of D , it is desired to conduct additional analyses, both to investigate the driving mechanisms behind its strong effect, but also to explore the effect of the factor outside the space of the factorial designs. This is briefly treated in Section 4.5. The results suggest that factor D should be the central parameter used for a simplified estimation of the overpressure. This is discussed further in Section 4.6.

According to the ANOVA, the effects of A , B , and C are also statically significant (P -value < 0.05) and contribute to the variation of overpressure roughly equally (in the order of 10 %). In Figure 16, signs of non-linearity were observed for the main effect of these factors. The non-linear behaviour was particularly pronounced for factor A . For this factor, the greatest overpressure was registered for the medium level. That is, its effect was positive between the low and medium levels, but it became negative between the medium and high levels. This indicates that increasing the value of A up to a certain optimal value will lead to greater overpressure, possibly due to a longer path for flame travel and turbulence

Table 5: ANOVA for the 3^{4-1} fractional factorial design.

Source	Sum of squares	Degrees of freedom	Mean square	F -statistic	P -value	Contribution
D	8,578	2	4,289	63.51	< 0.001	55.8 %
A	1,613	2	807	11.95	0.008	10.5 %
C	1,539	2	769	11.39	0.009	10.0 %
B	1,080	2	540	7.99	0.020	7.0 %
AD	1,298	4	324	4.80	0.044	8.4 %
CD	621	4	155	2.30	0.173	4.0 %
BD	244	4	61.1	0.90	0.517	1.6 %
Residual	405	6	67.5	–	–	2.6 %

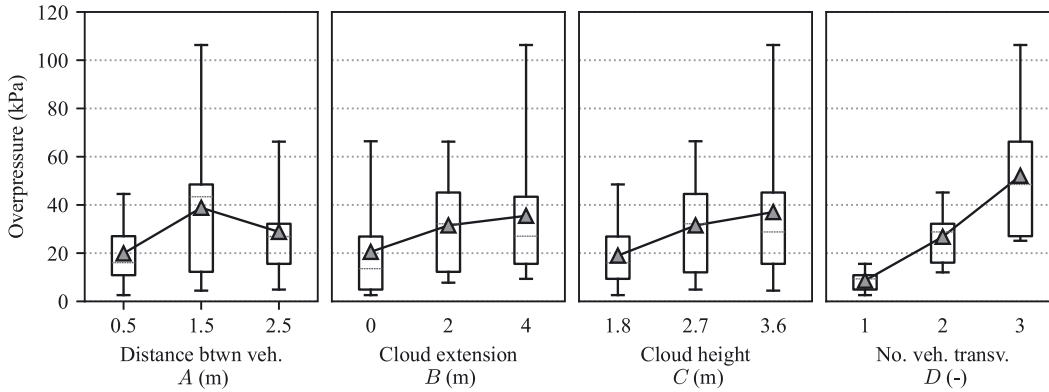


Figure 16: Plots of main effects obtained from the targeted 3^{4-1} fractional factorial design. The boxes extend from the 25th to the 75th percentile. The triangles represent the mean value.

generation in the recirculation regions between the vehicles. However, further increase beyond the optimal value will enable deceleration of the flame in the zones between vehicles, ultimately decreasing the maximum overpressure that can be achieved. Therefore, for sufficiently large values of A , the scenario could be treated as separate smaller explosions. Indeed, this is recognised by the MEM, in which obstructed areas separated by open and unobstructed regions of sufficient extent are considered as separate sources of blast, see e.g. [67].

Figure 16 shows that the main effect of factor B subsided as the factor increased. That is, the response changed more rapidly between the low and medium levels, while the change between medium and high levels was more subdued. This indicates that increasing B further might not lead to a significant increase in maximum overpressure. Two processes have been identified as the main reasons for this behaviour. First, for situations when the ignition point is located at the edge of the congested region, increasing the volume of flammable mixture behind the ignition point outside the congested region has the consequence of delaying venting of combustion products, which enables higher flame speed within the congested region. However, this phenomenon is only significant up to a certain volume of flammable material outside the congested region, possibly connected to the gas volume that is required to sustain combustion behind the ignition point until the flame front crosses the congested region. This process is not expected to have a strong influence in scenarios with central ignition. Secondly, as the flow ahead of the flame exits the congested region, it generates a zone with intense turbulence in the wake of the obstacles just outside the congested region. When the flame reaches this recirculation zone, it continues to accelerate for a short distance (which enables further pressure build-up) before decelerating. As B increases, more

flammable material is set into turbulent motion within the recirculation zone before ignition, which results in greater overpressure. However, once there is sufficient flammable material to cover the entire recirculation zone, no further increase of the overpressure is expected for greater values of B . However, more detailed research is needed to confirm the conceptual explanations discussed here.

The trend displayed by the effect of factor C (height of the gas cloud) was similar to that of B . The results indicate that the effect levels off after a certain value, so that further increase of C does not significantly enhance the maximum overpressure. The influence of the recirculation zone, as described above, is believed to be the driving process behind the effect of C .

The interactions effects AD , BD and CD were also included in the ANOVA. These interactions are also plotted in Figure 17. Overall, it appears that the effects of A , B , and C on the maximum overpressure is small when $D = 1$, while their influence increases for $D > 1$. Particularly, the distance between vehicles (factor A) had almost no effect for $D = 1$, while it had a much more significant (and non-linear) effect when $D = 2$ and $D = 3$. Moreover, the relative increase in overpressure between consecutive values of D is greatest for $A = 1.5$ m. The minor main effect of A when $D = 1$ was not unexpected, considering that, when $D = 1$, factor A is only relevant in the longitudinal direction, in conjunction with the previously identified minimal effect of factor E and interaction AE . An interesting observation for factors B and C is that the change between the medium and high values is largest for $D = 3$, which could indicate that the size of the recirculation zone (where flame acceleration outside the congested region may still be possible) increases for greater values of D .

While the effect of interactions AD , BD and CD could be discerned in Figure 17, only AD was found to be statistically

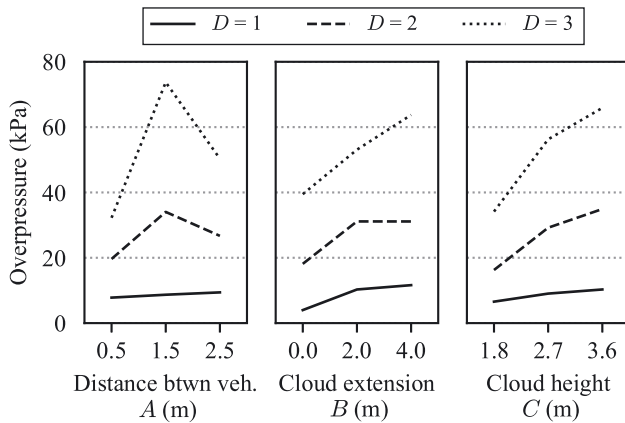


Figure 17: Two-factor interactions effects AD , BD and CD obtained from the targeted 3^{4-1} fractional factorial design.

significant (P -value < 0.05) in the ANOVA. In contrast, the high P -values associated with CD and BD indicate that it cannot be claimed with sufficient evidence that these interactions have a significant relationship with the variation of overpressure. However, it should be noted that this does not necessarily prove that there is no relationship. Instead, it implies that more data may be needed to confirm the effects of CD and BD . However, the analysis does suggest that the expected contributions of CD and BD to the variability of the overpressure are comparatively minor (less than 5%).

The fact that only one interaction was proven to be statistically significant as the main effects suggests that a more thorough investigation of the main effects may be carried out by disregarding the interaction effects. Future studies may benefit from implementing, for example, a one-factor-at-a-time approach, in which the factor of interest is varied over a large range of values with the other factors held constant.

4.5 Complementary analyses

4.5.1 Extended investigation of the effect of the number of vehicles

Situations in which either D or E exceed 3 may occur relatively frequently in traffic environments. Therefore, it is of interest to explore the effect of these factors outside the space evaluated by the factorial designs. The study presented in this subsection is not meant to be exhaustive but rather to inform about the potential expected behaviour and to open avenues for future research work.

The additional scenarios were analysed following a one-factor-at-a-time approach, whereby only D or E were varied, while all other parameters remained fixed. To investigate

the effect of D , five scenarios were analysed. These scenarios were defined by $A = 1$ m, $B = 2$ m, $C = 2.7$ m, and $E = 3$, while D was varied between 1 and 5. Similarly, four scenarios were analysed to study the effect of E , with $A = 0.5$ m, $B = 2$ m, $C = 1.8$ m, $D = 3$, and E varying between 1 and 4. The new models were created using the procedure and conditions described in Section 3.2.

The maximum overpressures from the additional scenarios are given in Figure 18. As expected, the maximum overpressure is shown to increase with increasing D . The relationship appears to be linear up to $D = 4$. However, the effect of D decreased between $D = 4$ and 5. That is, the effect of D appears to level off after a certain value of D , which was not previously discerned from the factorial designs. This may indicate that, as D increases, the effect of side venting may become more dominant than flame travel distance and no significant enhancement of maximum overpressure would be observed for greater values of D .

The value at which the effect of D plateaus may be related to E , as large values of E may delay side venting of the combustion products and vice versa. That is, it is reasonable to believe that the effect of D will level off sooner in scenarios with $E < 3$ compared to scenarios with $E > 3$. However, this cannot be demonstrated with the analyses conducted here, and further investigation is needed.

Additionally, Figure 18 shows that the influence of E on the maximum overpressure was minor. The increase in overpressure between $E = 1$ and $E = 2$ was 17%. Thereafter, the overpressure remained virtually unaffected. Thus, it can be expected that greater values of E will not produce greater

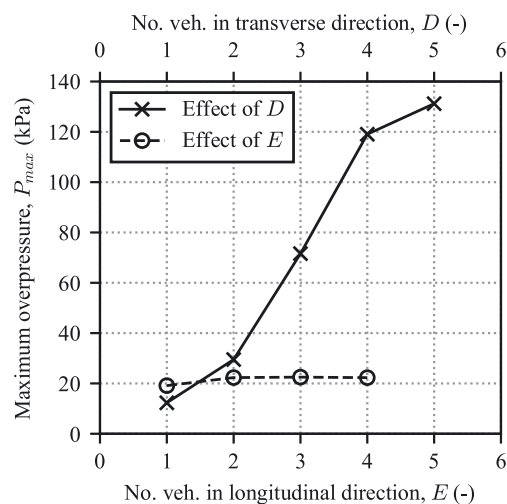


Figure 18: Maximum overpressure as a function of parameters D and E obtained from the complementary analyses. In the scenarios used for studying the effect of D : $A = 1$ m, $B = 2$ m, $C = 2.7$ m, $E = 3$. In the scenarios used for studying the effect of E : $A = 0.5$ m, $B = 2$ m, $C = 1.8$ m, $D = 3$.

overpressure. While the effect of E on the maximum overpressure was shown to be minor, this factor may still have a stronger influence on the positive impulse due to the larger gas cloud volume.

4.5.2 Effect of the wheels' orientation

It was previously speculated that the contrast between the effects of factors D and E may be connected to the orientation of the wheels. When the main direction of flow is perpendicular to the long side of the wheels, more intense turbulence is expected in their wake compared to the turbulence generated when the flow is parallel to the wheels. In general terms, greater D promotes flame propagation perpendicularly to the wheels, while E relates to flame propagation parallel to the wheels. Thus, increasing D has a more pronounced effect on the resulting overpressure.

To support this explanation, a simplified numerical investigation of the effect of the wheels' orientation on the overpressure from a confined deflagration was conducted. Four scenarios consisting of a gas cloud confined within a flat channel were studied. The scenarios were designed to be representative of the characteristics of the flow in the region underneath the vehicles. One scenario had no obstruction (S0), while the other three had two obstacles representing the wheels. The general geometry of the scenarios is given in Figure 19(a) and (b). The distance between the confining planes was set to 300 mm (equal to the ground clearance assumed in this study). All obstacles had the same depth

(300 mm). However, their shapes in the main plane of flow varied: i) rectangular shape oriented perpendicularly to the channel's main direction (S1: 500 × 200 mm); ii) rectangular shape oriented parallel to the channel's main direction (S2: 200 × 500 mm); and iii) square shape (S3: 500 × 500 mm). The CFD models were created using the procedure and conditions described in Section 3.2. The grid cell size was set to 50 mm.

The peak overpressure at a monitor point located at 3.0 m from the centre of the scenario is presented in Figure 19(d) for each scenario. The results were normalised relative to the peak overpressure in the S0 scenario. Clearly, the presence of the obstacles produced an increase of the peak overpressure for all the evaluated shapes. The greatest overpressure was obtained for the rectangular shape oriented perpendicularly to the flow (S1), with an increase of peak overpressure of 2.3 relative to the reference case. In contrast, the rectangular object placed parallel to the main direction of flow led to a noticeably smaller relative increase of overpressure (equal to 1.4). These results indicate that the flow perpendicular to the direction of traffic enhances pressure build-up due to the influence of the wheels. Indeed, signs of this phenomenon were previously observed by comparing Figure 8(d) and (f). Interestingly, the square obstacle (S0) produced a peak overpressure slightly smaller than that of the S1 configuration.

These results are consistent with other experimental and numerical studies, which have shown that the shape of the obstacle plays a significant role in the resulting

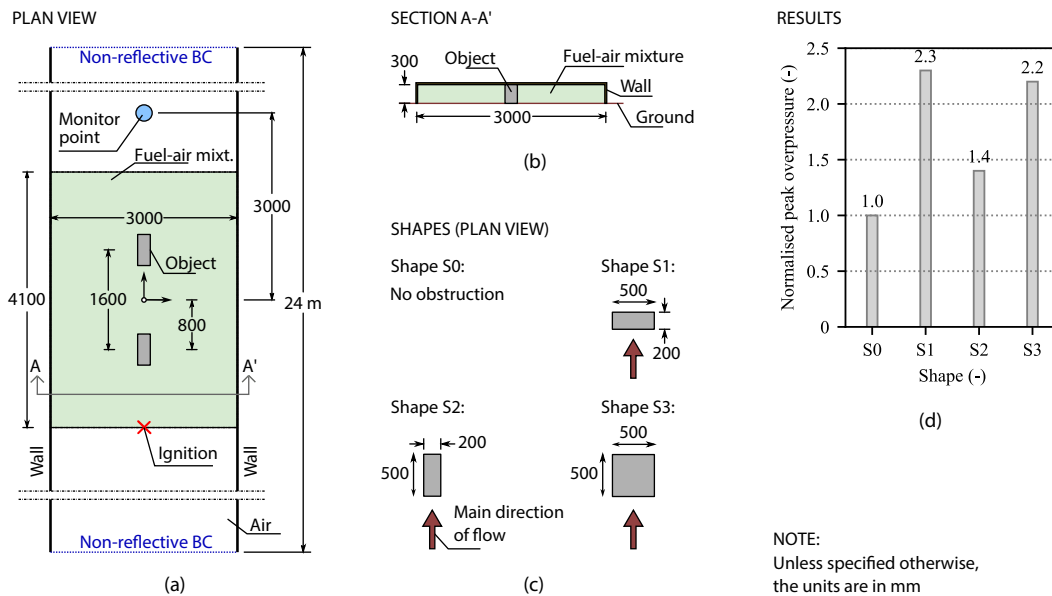


Figure 19: Study of the effect of the wheels' orientation: (a) Plan view, showcasing the S2 scenario (b) section view, showcasing the S2 scenario; (c) geometry of the obstacles; (d) maximum overpressure at the selected monitor point, normalised relative to the unobstructed scenario (S0).

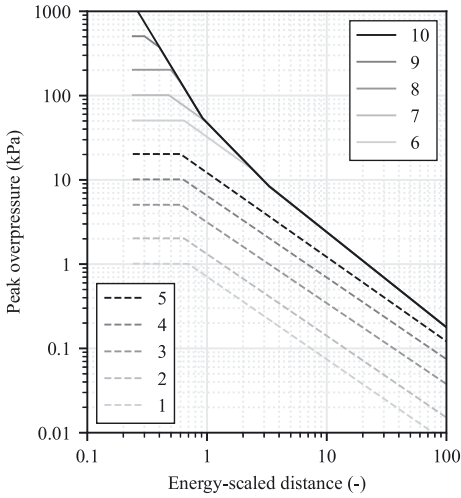


Figure 20: Side-on peak overpressure as a function of the energy-scaled distance and strength class, S . Plotted with equations in [73], based on [34].

overpressure in obstructed chambers [68–71]. Obstacles in the form of rectangular plates have been observed to yield greater overpressure compared to other shapes, such as square or cylindrical obstacles [68, 69]. It is also worth noting that the relative increase caused by the investigated shapes is remarkably similar to the drag coefficient of the corresponding two-dimensional rectangles [72].

4.6 Simplified estimate of the strength of VCEs in traffic environments

Among all the studied factors, the number of vehicles in the transverse direction, D , was found to have the strongest influence on the resulting overpressure: an increase in D consistently produced an increase in maximum overpressure. This suggests that factor D may be employed as the central parameter to estimate the overpressure of a VCE in a traffic environment. Since factors A , B and C also are significant, they should also be considered. However, it may not be necessary to consider the effect of varying A , B and C . Instead, as a conservative approach, it could be sufficient to adopt only their critical values that yield the greatest overpressure.

Such a simplified estimate of the overpressure may be achieved in different ways. An alternative would be to determine a numerical correlation to relate explosion overpressure to the scenario parameters. This approach was implemented in [40–42] for congested configurations within process plants. Another possibility would be to qualitatively relate the scenario parameters to a certain strength class or

severity level, similarly to the recommendations given in [39]. The calculated overpressure or strength class could then be used as an input to one of the existing simplified methods for estimating the blast load from VCEs, such as the MEM or the BST method.

To showcase how a simplified estimate of the VCEs strength could be achieved based on the parametric relationships observed in this study, a relationship between the most significant scenario parameters and the strength class in the MEM was derived. The MEM provides a chart for side-on peak overpressure as a function of the energy-scaled distance, containing a set of 10 curves for different strength class numbers, S , as shown in Figure 20. The strength class is assumed to depend on D , while the influence of the other significant factors is maximised. This is represented by Eq. (1). The critical values for factors A , B and C in Eq. (1) were taken from Figure 16.

$$S = f(D) \mid A = 1.5 \text{ m}, B \geq 2.0 \text{ m}, C \geq 2.7 \text{ m} \quad (1)$$

To define the function f in Eq. (1), the scenarios in Table 2 and Table 3 that fulfilled the imposed conditions for each value of D were first identified. Thereafter, the average value of maximum overpressure across the different scenarios, $\overline{P_{\max}}$, was determined. The closest strength class in the MEM was then found for each value of D . The resulting relationship between D and S are summarised in Table 6, in which P_{MEM} is the corresponding maximum overpressure in the MEM.

No scenario with $D \geq 4$ was included in the factorial designs. Hence, no strength class is proposed for such scenarios in Table 6. However, the complementary study presented in Section 4.5.1 suggests that the strength class for scenarios with $D \geq 4$ would be at least as large as that of the $D = 3$ scenario.

It should be noted that for a complete prediction of the blast load using the MEM, the combustion energy at the source of strong blast must be determined. The combustion energy influences the overpressure at a distance. The MEM relates the combustion energy to the gas volume at the source of blast. This topic is outside the scope of the present

Table 6: Proposed strength class for a group of vehicles based on the number of vehicles in the transverse direction, D . $\overline{P_{\max}}$ is the average maximum overpressure across the corresponding CFD scenarios. P_{MEM} is the maximum overpressure in the MEM.

D (-)	$\overline{P_{\max}}$ (kPa)	S (-)	P_{MEM} (kPa)
1	13	4	10
2	44	6	50
3	92	7	100

work. Nonetheless, a preliminary comparison between the CFD results and the prediction with the MEM is conducted for two selected scenarios: scenario 1–29 (1 vehicle) and scenario 1–32 (3×3 vehicles). For the calculation of the combustion energy, two different values of the gas volume at the source of blast were assumed: the total gas volume in the scenarios ($V_{gas,max}$); and a smaller volume equal to the volume of the congested region ($V_{gas,min}$). The volume $V_{gas,min}$ was calculated from the perimeter of the group of vehicles and a cloud height equal to 1.8 m [56]. The calculations with the MEM were done in accordance with [34] using the strength class in Table 6.

Figure 21 shows a comparison between the CFD results and the prediction with the MEM. For both scenarios, using the total gas volume resulted in a clear overprediction of peak overpressure at a distance. This was not unexpected, as only a portion of the total flammable mixture have the conditions to produce a blast with the assumed strength class. On the other hand, using $V_{gas,min}$ led both to underprediction (scenario 1–29) and overprediction (scenario 1–32) of the overpressure at a distance. For the analysed cases, the prediction with $V_{gas,min}$ produced an error in the order of $\pm 50\%$ with respect to the CFD results. Furthermore, the error in the prediction with the MEM for the scenario with 3×3 vehicles suggests that the assumed strength class ($S = 7$) should be applied only to a limited gas volume which is smaller than the congested region, while the remaining (and greater) gas volume in the congested region may be considered as a separate overall explosion with lower strength class. Hence, research concerning the volume of mixture contributing to blast generation is needed to complete the insights gained in this article to be able to formulate complete recommendations for implementing the MEM for

the environment of interest. This will be addressed in detail in future research.

5 Conclusions

This study evaluated the influence of relevant parameters on the strength of explosions of propane-air mixtures in a traffic environment using CFD analysis. The studied scenarios consisted of groups of vehicles arranged in different configurations engulfed by a stoichiometric vapour cloud. Two fractional factorial designs were employed to investigate the effects of the studied parameters. The aim was to understand and quantify the influence of relevant parameters on the maximum overpressure. Furthermore, the study investigated how the explosion strength could be estimated in a simplified manner based on the most significant parameters, with the intention of facilitating calculation of this important input for simplified methods such as the TNO Multi-Energy Method (MEM) for evaluation of vapour cloud explosions in a traffic environment.

The parameters examined in this study were the separation distance between vehicles, the dimensions of the gas cloud, the number of vehicles in the transverse and longitudinal directions, and the location of the ignition point. A large variation in explosion strength depending on the values of these parameters was observed (between 2 kPa and 106 kPa). However, in the scenarios producing the stronger explosions, the large values of overpressure were attained only in localised areas with small effect radius. This implies that the energy contributing to strong blast was limited in relation to the total congested gas volume.

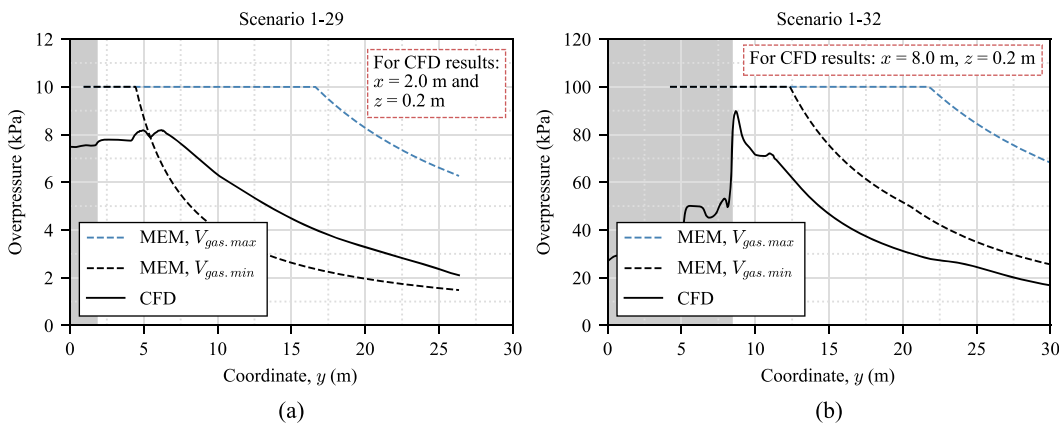


Figure 21: Comparison of overpressure-distance curves at selected paths between CFD analyses and predictions with the MEM. The shaded area represents the region occupied by the vehicles. The dashed lines are the prediction with the MEM using the total gas volume ($V_{gas,max}$, blue line) or the volume of the congested region ($V_{gas,min}$, black line). Following Table 6, the strength class was set to (a) $S = 4$; (b) $S = 7$.

The number of vehicles in the transverse direction (i.e. vehicles placed side by side) had the most significant effect on the explosion strength, while the number of vehicles in the longitudinal direction had the least impact among the studied parameters. This observation suggests that the number of lanes on a road has greater influence on the explosion strength than the length of the queue of vehicles. Additionally, carparks where vehicles park side by side have considerable potential for powerful explosions.

For the assumed vehicle geometry (width: 1.8 m \times length: 4.8 m), increasing the separation distance between vehicles from 0.5 to 1.5 m resulted in greater maximum overpressure. However, a decrease in overpressure was observed when this distance was further increased to 2.5 m. This may indicate that the flame travel distance across the congested area is initially dominant. However, after a certain value of the separation distance, the relief of pressure in the region between vehicles prevails, ultimately leading to overpressure decrease.

Increasing the volume of flammable mixture outside the congested region was shown to initially produce greater maximum overpressure. However, the effect of the gas volume declined after a certain volume, meaning that further increase of the gas volume would not lead to a significant enhancement of the overpressure.

Finally, the study proposed estimating the strength class for scenarios involving groups of vehicles based on a single parameter: the number of vehicle rows in the transverse direction. Preliminary recommendations for the estimation of the strength class number as a function of this parameter were given. However, more research is needed to confirm and expand these recommendations.

This article specifically focused on the strength class at the blast source. The study should be complemented with more detailed investigation of the amount of energy contributing to blast generation. This involves studying the effective volume of flammable mixture at the source of strong blast.

Moreover, a more thorough evaluation of the influence of the number of vehicles and the separation distance for values outside the range assumed in this work is needed. Finally, this study adopted a constant vehicle geometry, including a constant ground clearance. Hence, it would be beneficial to investigate the effect of varying those parameters on the resulting overpressure in future research.

Acknowledgments: The calculations were performed on two high-performance computing (HPC) clusters: *Vera*, provided by Chalmers e-Commons at Chalmers; and *Tetralith*, provided by the National Academic Infrastructure for

Supercomputing in Sweden (NAISS) and the Swedish National Infrastructure for Computing (SNIC).

Funding information: This work was financed by the Swedish Transport Administration; the Swedish Fortifications Agency; and the Swedish Civil Contingencies Agency. The authors are grateful for their support.

Author contributions: All authors have accepted responsibility for the entire content of this manuscript and consented to its submission to the journal, reviewed all the results and approved the final version of the manuscript. **FL:** writing (original draft), visualization, validation, software, methodology, investigation, formal analysis, conceptualization. **MJ:** writing (review & editing), supervision, project administration, methodology, funding acquisition, conceptualization. **JL:** writing (review & editing), supervision, project administration, methodology, funding acquisition, conceptualization. **MP:** writing (review & editing), supervision, methodology, conceptualization.

Conflict of interest: Authors state no conflict of interest.

Data availability statement: The datasets generated during and/or analysed during the current study are available from the corresponding author on reasonable request.

References

1. Guo J, Luo C. Risk assessment of hazardous materials transportation: a review of research progress in the last thirty years. *J Traffic Transp Eng Engl Ed* 2022;9:571–90.
2. Carol S, Vilchez JA, Casal J. Study of the severity of industrial accidents with hazardous substances by historical analysis. *J Loss Prev Process Ind* 2002;15:517–24.
3. Khan FI, Abbasi SA. Major accidents in process industries and an analysis of causes and consequences. *J Loss Prev Process Ind* 1999;12:361–78.
4. Eurostat [Internet]. Road freight transport of dangerous goods by type of dangerous goods and territorial coverage (tkm, vehicle-km, basic transport operations) - annual data. [cited 2024 Jun 07]. https://doi.org/10.2908/ROAD_GO_TA_DG.
5. Bubbico R, Ferrari C, Mazzarotta B. Risk analysis of LPG transport by road and rail. *J Loss Prev Process Ind* 2000;13:27–31.
6. Casal J. Evaluation of the effects and consequences of major accidents in industrial plants, 2nd ed. Amsterdam: Elsevier; 2018.
7. Bjerketvedt D, Bakke JR, van Wingerden K. Gas explosion handbook. Bergen: Gexcon; 1992.
8. Kang Y, Wu Z, Ma S, Zhao M, Li W. CFD-based assessment and visualization of the failure consequences of LPG tankers. *J Loss Prev Process Ind* 2023;82:105008.
9. Lyu S, Zhang S, Huang X, Peng S, Li J. Investigation and modeling of the LPG tank truck accident in Wenling, China. *Process Saf Environ Prot* 2022;157:493–508.
10. Yang D, Peng K, Zheng J, Xie B, Wang J, Xu B, et al. Consequences analysis of the LPG tank truck traffic accident: a case study of the Wenling explosion accident. *J Loss Prev Process Ind* 2024;87:105228.

11. Johansson M, Ansell A, Hallgren M, Leppänen J. Inventering av kunskapsbehov i byggbranschen med hänsyn till explosioner i en förtätad stadsmiljö (Inventory of knowledge needs in the construction industry regarding explosions in densified urban environments. In Swedish). Göteborg: Chalmers University of Technology; 2020.
12. Shirvill LC, Royle M, Roberts TA. Hydrogen releases ignited in a simulated vehicle refuelling environment. In: 2nd Int. Conference for hydrogen safety, San Sebastian, Spain; 2007: 11–3 pp.
13. Mishra S, Mishra KB. Numerical study of large-scale LNG vapour cloud explosion in an unconfined space. *Process Saf Environ Prot* 2021;149: 967–76.
14. Momferatos G, Giannisi SG, Toliás IC, Venetsanos AG, Vlyssides A, Markatos N. Vapor cloud explosions in various types of confined environments: CFD analysis and model validation. *J Loss Prev Process Ind* 2022;75:104681.
15. Hu Q, Qian X, Shen X, Zhang Q, Ma C, Pang L, et al. Investigations on vapor cloud explosion hazards and critical safe reserves of LPG tanks. *J Loss Prev Process Ind* 2022;80:104904.
16. Hansen OR, Hinze P, Engel D, Davis S. Using computational fluid dynamics (CFD) for blast wave predictions. *J Loss Prev Process Ind* 2010; 23:885–906.
17. Hansen OR, Johnson DM. Improved far-field blast predictions from fast deflagrations, DDTs and detonations of vapour clouds using FLACS CFD. *J Loss Prev Process Ind* 2015;35:293–306.
18. Li J, Hao H. Internal and external pressure prediction of vented gas explosion in large rooms by using analytical and CFD methods. *J Loss Prev Process Ind* 2017;49:367–81.
19. Shen R, Jiao Z, Parker T, Sun Y, Wang Q. Recent application of computational fluid dynamics (CFD) in process safety and loss prevention: a review. *J Loss Prev Process Ind* 2020;67:104252.
20. Jiao Y, Chen R, Wang K, Fan X, Liu F. Simulation of scenario characteristics of LPG tank explosion accident and its contribution to emergency planning: a case study. *J Loss Prev Process Ind* 2023;83: 105066.
21. Venetsanos AG, Baraldi D, Adams P, Heggem PS, Wilkening H. CFD modelling of hydrogen release, dispersion and combustion for automotive scenarios. *J Loss Prev Process Ind* 2008;21:162–84.
22. Venetsanos AG, Huld T, Adams P, Bartzis JG. Source, dispersion and combustion modelling of an accidental release of hydrogen in an urban environment. *J Hazard Mater* 2003;105:1–25.
23. Shi J, Li J, Zhang H, Xie B, Xie Z, Yu Q, et al. Real-time gas explosion prediction at urban scale by GIS and graph neural network. *Appl Energy* 2025;377:124614.
24. Shi J, Li J, Zhang H, Yan J. Towards physics-guided graph neural network for hydrogen gas explosion simulation at urban scale. *Appl Energy* 2025;401:126592.
25. Baraldi D, Kotchourko A, Lelyakin A, Yanez J, Middha P, Hansen OR, et al. An inter-comparison exercise on CFD model capabilities to simulate hydrogen deflagrations in a tunnel. *Int J Hydrogen Energy* 2009;34:7862–72.
26. Li YZ. Study of fire and explosion hazards of alternative fuel vehicles in tunnels. *Fire Saf J* 2019;110:102871.
27. Middha P, Hansen OR. CFD simulation study to investigate the risk from hydrogen vehicles in tunnels. *Int J Hydrogen Energy* 2009;34:5875–86.
28. To CW, Chow WK, Cheng FM. Numerical studies on explosion hazards of vehicles using clean fuel in short vehicular tunnels. *Tunn Undergr Space Technol* 2021;107:103649.
29. Li W, Shen X, Huang Z, Mao T, Hu Q, Ma C. Study of leakage and explosion hazard characteristics of a compressed natural gas at a gas station. *J Eng Phys Thermophys* 2024;97:387–96.
30. Makarov D, Verbecke F, Molkov V, Roe O, Skotenne M, Kotchourko A, et al. An inter-comparison exercise on CFD model capabilities to predict a hydrogen explosion in a simulated vehicle refuelling environment. *Int J Hydrogen Energy* 2009;34:2800–14.
31. Zhou C, Yang Z, Chen G, Li X. Optimizing hydrogen refueling station layout based on consequences of leakage and explosion accidents. *Int J Hydrogen Energy* 2024;54:817–36.
32. Yang Z, Chen Z, Han X, Chen G, Wang X. Numerical and experimental studies on the evolution characteristics of high-pressure hydrogen leakage and explosion accidents in hydrogen refueling stations. *Int J Hydrogen Energy* 2025;142:580–95.
33. Wang K, Xu S, Zhou M, Shi T. Computational insights into evolution mechanism of hydrogen vapor cloud explosion and expanding resistant capabilities in oil-hydrogen refueling station. *Int J Hydrogen Energy* 2025;115:310–25.
34. van den Berg AC. The multi-energy method: a framework for vapour cloud explosion blast prediction. *J Hazard Mater* 1985;12:1–10.
35. Baker QA, Tang MJ, Scheier EA, Silva GJ. Vapor cloud explosion analysis. *Process Saf Prog* 1996;15:106–9.
36. Tang MJ, Baker QA. A new set of blast curves from vapor cloud explosion. *Process Saf Prog* 1999;18:235–40.
37. Puttock JS. T7-5 – developments in the congestion assessment method for the prediction of vapour-cloud explosions. In: Pasman HJ, Fredholm O, Jacobsson A, editors. Proceedings of the 10th international symposium on loss prevention and safety promotion in the process industries. Stockholm: Elsevier Science B.V.; 2001. p. 1107–33.
38. Committee for the Prevention of Disasters. Methods for the calculation of physical effects [‘yellow book’]. The Hague: Ministerie van VROM; 2005.
39. Kinsella KG. A rapid assessment methodology for the prediction of vapour cloud explosion overpressure. International conference and exhibition on safety, health and loss prevention in the oil. Singapore: Chemical and process industries; 1993.
40. Eggen JBMM. GAME: development of guidance for the application of the multi-energy method. Rijswijk: TNO Prins Maurits Laboratory; 1998.
41. Li J, Abdel-jawad M, Ma G. New correlation for vapor cloud explosion overpressure calculation at congested configurations. *J Loss Prev Process Ind* 2014;31:16–25.
42. Shi Y, Xie C, Li Z, Ding Y. A quantitative correlation of evaluating the flame speed for the BST method in vapor cloud explosions. *J Loss Prev Process Ind* 2021;73:104622.
43. Gexcon AS. FLACS-CFD v22.1 user’s manual 2022.
44. Montgomery DC. Design and analysis of experiments, 8th ed. Hoboken, NJ: John Wiley & Sons, Inc; 2013.
45. Lozano F. Explosions in urban environments: modelling of gas explosions and risk of premature shear failure in reinforced concrete structures [Licentiate thesis]. Gothenburg: Chalmers University of Technology; 2023.
46. Hansen OR, Gavelli F, Davis SG, Middha P. Equivalent cloud methods used for explosion risk and consequence studies. *J Loss Prev Process Ind* 2013;26:511–27.
47. Tam VHY, Tan F, Sawides C. A critical review of the equivalent stoichiometric cloud model Q9 in gas explosion modelling. *Eng* 2021;2: 156–80.
48. Lozano F, Johansson M, Leppänen J, Plos M. CFD modelling of LPG dispersion in a road environment. *Chem Eng Trans* 2024;111:313–8.
49. Bai Y, Wu J, Sun Y, Cai J, Cao J, Pang L. BN & CFD-Based quantitative risk assessment of the natural gas explosion in utility tunnels. *J Loss Prev Process Ind* 2022;80:104883.

50. Wang Q, Sun Y, Shu C-M, Jiang J, Zhang M, Wang Q, et al. Effect of separation distance on gas dispersion and vapor cloud explosion in a storage tank farm determined using computational fluid dynamics. *J Loss Prev Process Ind* 2020;68:104282.
51. Van den Schoor F, Middha P, Van den Bulck E. Risk analysis of LPG (liquefied petroleum gas) vehicles in enclosed car parks. *Fire Saf J* 2013; 57:58–68.
52. Lozano F, Johansson M, Leppänen J, Plos M. Effect of partial confinement on vapour cloud explosions on a road: a numerical study. In: *Proceedings of the 15th international conference on shock & impact loads on structures*. Gothenburg; 2025. 286–97 pp.
53. Alvarsson O, Jansson J. Jämförelsestudie av riskbedömningar avseende vägtransport av farligt gods (Comparison study of risk analyses regarding road transport of hazardous materials. In Swedish) [M.Sc. thesis]. Lund: Lund University; 2016.
54. Dahlén E. Inventory of knowledge needs with regard to explosion loading in a densified urban environment [M.Sc. thesis]. Gothenburg: Chalmers University of Technology; 2019.
55. Energigas Sverige [Internet]. FAQ om Gasol. [cited 2024 Jun 07]. <https://www.energigas.se/fakta-om-gas/gasol/faq-om-gasol/>
56. Pitblado R, Alderman J, Thomas JK. Facilitating consistent siting hazard distance predictions using the TNO multi-energy model. *J Loss Prev Process Ind* 2014;30:287–95.
57. Hjertager BH. Computer simulation of turbulent reactive gas dynamics. *Model Identif Control* 1984;5:211–36.
58. Hjertager BH. Computer modelling of turbulent gas explosions in complex 2D and 3D geometries. *J Hazard Mater* 1993;34:173–97.
59. Arntzen BJ. Modelling of turbulence and combustion for simulation of gas explosions in complex geometries [Doctoral dissertation]. Trondheim: Norwegian University of Science and Technology (NTNU); 1998.
60. Patankar SV, Spalding DB. A calculation procedure for the transient and steady-state behaviour of shell-and-tube heat exchangers. In: Afgan NH, Schhinder EV, editors. *Heat exchangers: design and theory Sourcebook*. New York: McGraw-Hill; 1974:155–76 pp.
61. Sha WT, Launder BE. A model for turbulent momentum and heat transport in large rod bundles. Lemont: Argonne National Laboratory; 1979.
62. Launder B, Spalding DB. The numerical computation of turbulent flow computer methods. *Comput Methods Appl Mech Eng* 1974;3: 269–89.
63. Lozano F. Gas explosion simulations in a traffic environment: grid sensitivity analysis and choice of grid resolution. Gothenburg: Chalmers University of Technology; 2024.
64. van Wingerden CJM. Experimental study of the influence of obstacles and partial confinement on flame propagation, part II. Rijswijk: TNO Prins Maurits Laboratory; 1984.
65. van Wingerden CJM. Experimental investigation into the strength of blast waves generated by vapor cloud explosions in congested areas. In: *6th Int. Symp. on loss prevention and safety promotion in the process industries*. Oslo; 1989.
66. Middha P. Development, use, and validation of the CFD tool FLACS for hydrogen safety studies [Doctoral dissertation]. Bergen: University of Bergen; 2010.
67. van den Berg AC, Mos AL. Research to improve guidance on separation distance for the multi-energy method (RIGOS). TNO Prins Maurits Laboratory; 2005.
68. Park DJ, Green AR, Lee YS, Chen Y-C. Experimental studies on interactions between a freely propagating flame and single obstacles in a rectangular confinement. *Combust Flame* 2007;150: 27–39.
69. Ibrahim SS, Masri AR. The effects of obstructions on overpressure resulting from premixed flame deflagration. *J Loss Prev Process Ind* 2001;14:213–21.
70. Li Y, Chen P, Bi M, Gao W. Premixed methane/air flame propagating in an obstructed chamber with different BRs and spatial configurations. *J Loss Prev Process Ind* 2017;47:66–71.
71. Nguyen T, Strebinger C, Bogin GE, Brune J. A 2D CFD model investigation of the impact of obstacles and turbulence model on methane flame propagation. *Process Saf Environ Prot* 2021;146: 95–107.
72. Leishman JG. Bluff body flows. In: *Introduction to aerospace flight vehicles*. Florida: Embry-Riddle Aeronautical University; 2023.
73. Johansson M. Beräkningsstöd: Gasexplosion i det fria (gas explosions in the open. In Swedish). Karlstad: Myndigheten för samhällsskydd och beredskap; 2017.